NASA TECHNICAL MEMORANDUM

NASA TM X-3501

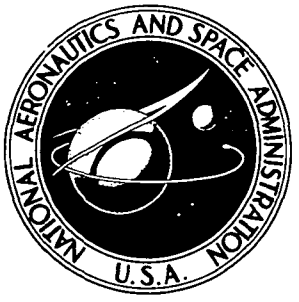

NASA TM X-3501

TAIL CONTRIBUTION TO THE DIRECTIONAL AERODYNAMIC CHARACTERISTICS OF A 1/6-SCALE MODEL OF THE ROTOR SYSTEMS RESEARCH AIRCRAFT WITH A TAIL ROTOR

Raymond E. Mineck

Langley Directorate,
U.S. Army Air Mobility R&D Laboratory

Langley Research Center
Hampton, Va. 23665

NATIONAL AERONAUTICS AND SPACE ADMINISTRATION • WASHINGTON, D. C. • MAY 1977

1. Report No.	2. Government Accession No.	3. Recipient's Catalog No.
NASA TM X-3501		

4. Title and Subtitle	5. Report Date
TAIL CONTRIBUTION TO THE DIRECTIONAL AERODYNAMIC CHARACTERISTICS OF A 1/6-SCALE MODEL OF THE ROTOR SYSTEMS RESEARCH AIRCRAFT WITH A TAIL ROTOR	May 1977
	6. Performing Organization Code

7. Author(s)	8. Performing Organization Report No.
Raymond E. Mineck	L-11271
	10. Work Unit No. 505-10-21-05

9. Performing Organization Name and Address	11. Contract or Grant No.
Langley Directorate, USAAMRDL NASA Langley Research Center Hampton, VA 23665	
	13. Type of Report and Period Covered: Technical Memorandum

12. Sponsoring Agency Name and Address	14. Army Project No.
National Aeronautics and Space Administration Washington, DC 20546 and U.S. Army Air Mobility R&D Laboratory Moffett Field, CA 94035	1F161102AH45

15. Supplementary Notes

16. Abstract

This report presents the results of a wind-tunnel investigation to determine the tail contribution to the directional aerodynamic characteristics of a 1/6-scale model of the rotor systems research aircraft (RSRA) with a tail rotor. No main rotor was used during the investigation. Data were obtained with and without the tail rotor over a range of sideslip angle and over a range of rotor collective pitch angle. The model with the tail rotor was tested at several advance ratios with and without thrust from the auxiliary thrust engines on the RSRA fuselage.

Increasing the space between the tail-rotor hub and the vertical tail reduces the tail-rotor torque required at moderate to high rotor thrust. Increasing the exit dynamic pressure of the auxiliary thrust engines decreases the tail contribution to the static directional stability. The tail-rotor thrust and its interference provide a positive increment to the static directional stability. The tail contribution increases with forward speed. The adverse yawing moment of the airframe would strongly affect the thrust required of the tail rotor when the helicopter is hovering in a crosswind.

17. Key Words (Suggested by Author(s))	18. Distribution Statement
RSRA (rotor systems research aircraft) Tail rotors	Unclassified - Unlimited Subject Category 02

19. Security Classif. (of this report)	20. Security Classif. (of this page)	21. No. of Pages	22. Price*
Unclassified	Unclassified	39	$4.00

*For sale by the National Technical Information Service, Springfield, Virginia 22161

TAIL CONTRIBUTION TO THE DIRECTIONAL AERODYNAMIC CHARACTERISTICS OF A 1/6-SCALE MODEL OF THE ROTOR SYSTEMS RESEARCH AIRCRAFT WITH A TAIL ROTOR

Raymond E. Mineck*
Langley Research Center

SUMMARY

This report presents the results of a wind-tunnel investigation to determine the tail contribution to the directional aerodynamic characteristics of a 1/6-scale model of the rotor systems research aircraft (RSRA) with a tail rotor. No main rotor was used during the investigation. Data were obtained with and without the tail rotor over a range of sideslip angle and over a range of rotor collective pitch angle. The tail rotor was tested at several advance ratios with and without thrust from the auxiliary thrust engines on the RSRA fuselage.

Increasing the space between the tail-rotor hub and the vertical tail reduces the tail-rotor torque required at moderate to high rotor thrust. Increasing the exit dynamic pressure of the auxiliary thrust engines decreases the tail contribution to the static directional stability. The tail-rotor thrust and its interference provide a positive increment to the static directional stability. The tail contribution increases with forward speed. The adverse yawing moment of the airframe would strongly affect the thrust required of the tail rotor when the helicopter is hovering in a crosswind.

INTRODUCTION

Helicopter tail rotors operate in a very complex flow field. The flow field becomes more complex when auxiliary propulsion devices such as turbofans or propellers are added to the helicopter or when the helicopter is operated in ground effect. Because these flow fields are complex, it is difficult to predict analytically the effects of the rotor wake or auxiliary propulsion devices. The effects often must be determined experimentally. The results of an investigation of tail-rotor operations in the wake of a main rotor operating in ground effect are presented in reference 1. The results of an investigation to determine the tail contribution to the directional aerodynamic characteristics of a 1/6-scale model of the rotor systems research aircraft (RSRA) are given in the present report. The model was tested with and without a tail rotor and with and without thrust from the auxiliary thrust engines on the RSRA fuselage. No main rotor was used in the investigation. Force and moment data on the airframe and tail assembly and tail-rotor blade flapping were

---

*Langley Directorate, U.S. Army Air Mobility R&D Laboratory.

obtained. Results obtained for the model with and without the main rotor but with no tail rotor may be found in reference 2.

The RSRA is a unique helicopter designed to obtain accurate data for rotorcraft theory development and to evaluate advanced rotor systems. It is equipped with a removable variable-incidence wing and removable auxiliary thrust engines. The RSRA may be flown as a fixed-wing aircraft, a compound helicopter, or a pure helicopter. Additional details of the RSRA may be found in reference 3.

SYMBOLS

The units used for the physical quantities defined in this paper are given in the International System of Units (SI) and parenthetically in U.S. Customary Units. Measurements and calculations were made in the U.S. Customary Units. Conversion factors relating the two systems are presented in reference 4.

The longitudinal data for the tail assembly are resolved in the stability-axis system and the lateral data for the tail assembly and airframe are resolved in the body-axis system. The data for the tail rotor are resolved in the rotor-shaft-axis system. The moment reference center for the tail and airframe data was located 3.81 cm (1.50 in.) behind and 35.14 cm (13.83 in.) below the main rotor hub. This moment reference center for the RSRA is the same as that used in references 3 and 5. The moment reference center for the tail-rotor data was the intersection of the model center line and the tail-rotor shaft. Sign conventions and nomenclature for the various measurements are shown in figure 1.

A tail-rotor disk area, 0.228 m^2 (2.45 ft^2)

a_0 tail-rotor coning angle, deg

a_{1s} tail-rotor longitudinal flapping angle, deg

b number of blades, four

b_w 1/6-scale wing span, 228.60 cm (90.00 in.)

b_{1s} tail-rotor lateral flapping angle, deg

$C_{D,t}$ tail-assembly drag coefficient, $\dfrac{\text{Tail drag}}{q_\infty S}$

$C_{L,t}$ tail-assembly lift coefficient, $\dfrac{\text{Tail lift}}{q_\infty S}$

$C_{l,t}$ tail-assembly rolling-moment coefficient, $\dfrac{\text{Tail rolling moment}}{q_\infty S b_w}$

$C_{m,t}$ tail-assembly pitching-moment coefficient, $\frac{\text{Tail pitching moment}}{q_\infty S \bar{c}}$

C_n airframe yawing-moment coefficient, $\frac{\text{Airframe yawing moment}}{q_\infty S b_w}$

$C_{n,t}$ tail-assembly yawing-moment coefficient, $\frac{\text{Tail yawing moment}}{q_\infty S b_w}$

$\left(C_{n_\beta}\right)_t$ tail contribution to the static directional stability, $\frac{dC_{n,t}}{d\beta}$

C_Q/σ tail-rotor torque coefficient, $\frac{Q}{\rho A V_T^2 R \sigma}$

C_T/σ tail-rotor thrust coefficient, $\frac{T}{\rho A V_T^2 \sigma}$

C_Y airframe side-force coefficient, $\frac{\text{Airframe side force}}{q_\infty S}$

$C_{Y,t}$ tail-assembly side-force coefficient, $\frac{\text{Tail side force}}{q_\infty S}$

c tail-rotor blade chord, 0.051 m (0.167 ft)

$\bar{c}$ 1/6-scale wing mean aerodynamic chord, 42.34 cm (16.67 in.)

Q tail-rotor torque, N-m (lbf-ft)

q_e dynamic pressure at fan exit, Pa (lbf/ft^2)

q_∞ free-stream dynamic pressure, Pa (lbf/ft^2)

R tail-rotor radius, 0.269 m (0.883 ft)

S wing area, 0.955 m^2 (10.277 ft^2)

T tail-rotor thrust, N (lbf)

V_∞ free-stream velocity, m/sec (ft/sec)

V_T tail-rotor tip speed, ΩR, m/sec (ft/sec)

y tail-rotor lateral displacement, m (ft)

α angle of attack, deg

β angle of sideslip, deg

$\Delta C_{n,t}$ tail-removed yawing-moment coefficient, Rotor-on $C_{n,t}$ - Rotor-off $C_{n,t}$

$\Delta \frac{C_T}{\sigma}$ tail-removed tail-rotor thrust coefficient, $\frac{\text{Rotor-on tail side force - Rotor-off tail side force}}{\rho A V_T^2 \sigma}$

$\Delta C_{Y,t}$ tail-removed side-force coefficient, Rotor-on $C_{Y,t}$ - Rotor-off $C_{Y,t}$

δ_3 pitch-flap coupling, -45°

η ratio of tail-rotor thrust required to hover in a 30-knot wind to thrust required to hover with no wind

θ_c tail-rotor collective pitch angle, deg

μ tail-rotor advance ratio, $\frac{V_\infty}{V_T}$

ρ free-stream density, kg/m^3 ($slugs/ft^3$)

σ tail-rotor solidity, $\frac{bcR}{A}$

ψ tail-rotor azimuth angle, deg

Ω tail-rotor rotational speed, rad/sec

Model components:

F tail cone and ventral fin

J auxiliary thrust jets

T tail-rotor motor fairing

V vertical tail

Abbreviations:

B.L. buttock line

F.S. fuselage station

W.L. water line

MODEL AND APPARATUS

The general rotor model system (GRMS) in the Langley V/STOL tunnel was used in this investigation. The external configuration was a 1/6-scale model of the RSRA. A detailed three-view sketch and an internal component layout of the model are presented in figure 2. The dimensions and areas of the model components are listed in table I.

The tail rotor, motor, and motor fairing were removable from the vertical tail. The vertical tail was removable from the tail cone. A strain-gage balance was used to measure the loads on the tail rotor, vertical tail, and tail cone from fuselage station 231.78 cm (91.25 in.) aft. At that point, a 0.28-cm (0.11-in.) unsealed gap in the tail cone allowed clearance for balance deflections.

The tail rotor used in this investigation had four blades on a hub that was articulated in pitch and flap directions only. The tail rotor had a pitch-flap coupling δ_3 of -45°, a solidity σ of 0.240, and a diameter of 53.84 cm (21.20 in.). The total twist of the blades from the center of rotation was -4°. Looking forward, the tail rotor was mounted on the left side of the vertical tail with a top-blade-aft direction of rotation. A 14.9-kW (20-hp) variable-speed electric motor enclosed in an airfoil-shaped housing was mounted on the right side of the vertical tail. The tail-rotor hub was located at fuselage station 299.29 cm (117.83 in.) and water line 117.07 cm (46.09 in.). Two lateral hub positions were investigated: (1) 10.16 cm (4.00 in.) from the center line of the model (the scaled location for the RSRA tail rotor (y/R = 0.40)) and (2) 16.27 cm (6.41 in.) from the center line (y/R = 0.64). One blade was instrumented for blade flapping angle at the blade hinge. Rotor speed and blade azimuth position were measured by means of magnetic pickups. The blade collective pitch angle was measured with a potentiometer. The collective pitch angle is the angle set by the swash plate. The actual blade pitch would be different because of the pitch-flap coupling.

Two removable auxiliary thrust engine nacelles were mounted on the fuselage. Each nacelle contained a removable fan to simulate the jet thrust. These fans, nacelles, and engine pylon fairings were the same as those used in reference 5. The engine pylon fairings were the "modified minimum fairings." (See fig. 2 of ref. 5.)

Each fan had a stator and a rotor. A ring of turbine blades was attached to the rotor. Dry, high-pressure air directed onto the turbine blades drove the fan to produce thrust. Each nacelle had one static-pressure orifice and three total-pressure probes mounted in the fan exit position of the engine. The three total-pressure probes were manifolded together. A pressure transducer was used to measure the difference between the total pressure in the manifold and the static pressure to obtain an average reference dynamic pressure at the exit. This exit dynamic pressure and the free-stream dynamic pressure were used to calibrate the engine thrust.

A photograph of the model in the Langley V/STOL tunnel is shown in figure 3. The model was mounted on a strain-gage balance supported by a special model support system which allowed high angles of attack and sideslip. This

sting model support system kept the model near the center line of the tunnel for pitch, yaw, and roll excursions. High-pressure air was piped into the model from an air plenum mounted directly below the total-loads balance. The plenum was fed by an air line running through the center of the sting. A reverse double coil in this air line minimized pressure effects of the air line crossing the total-loads balance.

TEST CONDITIONS AND CORRECTIONS

This investigation was conducted in the Langley V/STOL tunnel, which is a closed-circuit atmospheric tunnel with a 4.42-m (14.50-ft) by 6.63-m (21.75-ft) test section. Tunnel speed was varied from 0 to 130 knots. All testing was conducted with the model close to the center line of the test section.

The auxiliary engine thrust, measured on the total-loads balance, was calibrated statically as a function of the exit dynamic pressure. However, at forward speeds the exit dynamic pressure should be equal to the free-stream dynamic pressure when the engine produces no thrust. To account for this, the free-stream dynamic pressure is subtracted from the exit dynamic pressure and the result is used in the static calibration. (See fig. 4.)

The model was tested with the tail rotor on and off. For the tail-rotor-off tests, the angle of attack and angle of sideslip were varied for several model configurations to establish a baseline for determining the rotor effects. For the tail-rotor-on tests, angle of sideslip and tail-rotor collective pitch angle were varied at several wind speeds with and without thrust being produced by the auxiliary thrust engines. In addition, at hover two tail-rotor hub positions were tested. For all tail-rotor tests the nominal tip speed was 213 m/sec (700 ft/sec).

The tail-rotor collective pitch angle was measured by a potentiometer on the drive train of the swash-plate actuator. There was some play in the drive train which resulted in a hysteresis in the measurements for collective pitch. Therefore, these data should be used with caution.

The tail balance measured the loads on both the vertical tail and the tail rotor. The loads on the vertical tail were estimated from the results obtained with the tail rotor removed. The loads on the tail rotor were computed by subtracting the loads computed for the vertical tail from the loads measured on the tail balance and neglecting the interference of the tail rotor on the vertical tail.

Both static and dynamic data were recorded during the tests. The static data, recorded on a digital data-acquisition system, consisted of averaged values taken from the strain-gage balance in addition to engine exit pressure, model attitude, rotor speed, blade collective pitch angle, and wind-tunnel test conditions. The dynamic data, recorded on an oscillograph, consisted of blade flapping and blade azimuth angle. The values for blade flapping are referenced to the steady values obtained at 0° collective pitch in hover with the rotor

turning at its nominal speed. These data have been analyzed into steady and oscillatory components.

Corrections have been made to the data for the interference on the tail from the model support system. The tail-rotor-on data have been corrected for the effect of the motor fairing using the tail-rotor-off data from figures 5 and 6. No corrections were made for the effect of the tunnel walls because of the small size of the tail rotor relative to the test section.

PRESENTATION OF RESULTS

The results of the wind-tunnel investigation are presented in coefficient form. The rotor data have been nondimensionalized by the rotor disk area and the rotor tip speed. The rotor data are resolved in the rotor-shaft-axis system with the moment reference center at the intersection of the tail-rotor shaft and the center line of the model. The airframe and tail data have been nondimensionalized by the 1/6-scale wing area, span, and mean aerodynamic chord and the free-stream dynamic pressure, even though the wing was not used in this investigation. Using the wing dimensions will permit direct comparison of these results with those of references 3 and 5. The tail longitudinal data are resolved in the stability-axis system and the tail and airframe lateral data in the body-axis system. The results are presented as follows:

DISCUSSION OF RESULTS

Aerodynamic Characteristics of Tail Assembly Without Tail Rotor

The model was tested with the tail rotor removed to determine the aerodynamic contribution of each tail component. The effect of the various tail components on the longitudinal aerodynamic characteristics is presented in figure 5. The vertical tail produced a destabilizing increment to the longitudinal stability. The tail-rotor motor fairing acted like a horizontal tail to provide a stabilizing increment to the longitudinal stability. Since the fairing is not present on the RSRA, the effect of adding the fairing has been removed from the rotor-on data. The effect of the various tail components on the lateral aerodynamic characteristics is presented in figure 6. The ventral fin provides static directional stability and negative effective dihedral. Adding the vertical tail increases the static directional stability and

provides positive effective dihedral. The tail-rotor motor fairing decreases both the static directional stability and the effective dihedral. Because the motor fairing is not present on the RSRA, the increment in $C_{n,t}$ and $C_{Y,t}$ due to the motor fairing has been removed from the rotor-on data.

The effect of angle of attack on the lateral aerodynamic characteristics is presented in figure 7. The static directional stability parameter $\left(C_{n_\beta}\right)_t$ varies from 0.0042/deg to 0.0019/deg as the angle of attack increases from -5° to 10°. This occurs because the amount of the vertical tail exposed to the free stream decreases as the angle of attack increases.

Aerodynamic Characteristics of Tail Rotor

For a pusher tail rotor, such as the one used in the present investigation, the lateral spacing between the hub and vertical tail affects the inflow and consequently the thrust and torque of the tail rotor. The effect of lateral spacing on the tail-rotor aerodynamic characteristics is presented in figure 8. Increasing the space between the tail-rotor hub and the vertical tail increases the torque required at low thrust coefficients and reduces the torque required at moderate to high thrust coefficients (fig. 8(a)). The effect on the rotor coning angle is very small (fig. 8(b)). The effect of advance ratio (forward speed) on the tail-rotor aerodynamic characteristics is presented in figure 9. In general, the thrust coefficient increased with forward speed at positive collective pitch angles and the torque decreased with forward speed at moderate thrust coefficients and advance ratios greater than 0.09. The rotor coning angle and longitudinal flapping angle increase with rotor collective pitch (fig. 9(b)). The increase in longitudinal flapping is larger at the higher forward speeds. The effect of collective pitch on the lateral flapping angle was mixed.

Aerodynamic Characteristics of Tail Assembly With Tail Rotor

The forces on the tail rotor are proportional to the rotor tip speed squared. The forces on the vertical tail are proportional to the free-stream velocity squared (or dynamic pressure). From these relations, the coefficients C_T/σ and $C_{Y,t}$ are formed. Both coefficients are presented since both are useful.

The effect of tail-rotor collective pitch on the tail-assembly side-force and yawing-moment coefficients is presented in figure 10. Since the rotor thrust was approximately linear with collective pitch, the side-force and yawing-moment coefficients of the tail assembly were also approximately linear with collective pitch. The slope of the side-force-coefficient curve varies with the inverse of the advance ratio squared $1/\mu^2$. This was expected since both the coefficient $C_{Y,t}$ and the inverse of the advance ratio squared are proportional to the free-stream dynamic pressure.

The variation of tail-assembly loads with angle of sideslip is presented in figure 11 for several advance ratios with and without the auxiliary engine thrust. The coefficients include the forces on both the vertical tail and the tail rotor without engine thrust. The tail contribution to the directional stability without auxiliary engine thrust increases as the advance ratio increases from 0.09 to 0.19, but changes very little as the advance ratio increases from 0.19 to 0.27 (fig. 11(a)). Similarly, with the auxiliary engine thrust (fig. 11(b)), there is little change as the advance ratio increases from 0.19 to 0.27. The large separation between the curves of figure 11(a) is due to the differences in collective pitch setting and in free-stream dynamic pressure.

The variation of rotor flapping angle with angle of sideslip is presented in figure 12 for the same advance ratios and other conditions of figure 11. In general, the coning angle decreases with increasing positive angle of sideslip because the rotor-disk angle of attack and consequently the thrust decrease with angle of sideslip. At a given advance ratio, the variation of longitudinal flapping angle with angle of sideslip is small, and the variation of lateral flapping angle is mixed. The large scatter in some of the data is associated with difficulties in reading the oscillograph trace accurately.

The effect of angle of sideslip on the tail-assembly loads for two values of auxiliary engine thrust $\left(q_e/q_\infty\right)$ is presented in figure 13. Increasing the engine thrust decreases slightly the static directional stability for either advance ratio. This is similar to the results found in references 3 and 5.

The variation of rotor flapping angles with angle of sideslip is presented in figure 14 for the conditions presented in figure 13. The effects are generally small and the scatter makes it difficult to draw any conclusions.

The results at forward speeds with the tail rotor include the effects of the empennage, the tail rotor, and the interference between the empennage and the tail rotor. To calculate the effects of the tail rotor and the interference, the contribution of the empennage can be removed from the rotor-on data. The results of this calculation are presented in figure 15. As previously mentioned, rotor thrust should decrease with increasing angle of sideslip. The rotor thrust and interference $\Delta \frac{C_T}{\sigma}$ decrease with increasing positive angle of sideslip. The thrust and interference decrease more rapidly as the forward speed increases. The tail-rotor thrust and its interference provide a positive increment to the static directional stability at $\mu = 0.19$ and $\mu = 0.27$. The tail contribution to static directional stability increases with forward speed.

New helicopters are being designed to survive the loss of the tail rotor. One of the methods of designing the vertical tail for such an incident, described in reference 6, requires aerodynamic characteristics for the fuselage over a wide range of sideslip angle. Prediction of fuselage aerodynamics is difficult outside the range of angles over which linear aerodynamic theory can be applied. Some experimental results, such as those in reference 7, are available; however, they are often configuration dependent.

The RSRA was tested over a wide range of sideslip angle in the investigation described in reference 5. The vertical tail was the shortened vertical tail. The results from reference 5 for the vertical tail on and off are presented in figure 16, along with results extrapolated to the full-span vertical tail. As was found in reference 7, the peak yawing moment with the vertical tail on occurs at 110° of sideslip. This adverse yawing moment will strongly affect the thrust required of the tail rotor when the helicopter is hovering in a crosswind. The change in yawing moment in a 30-knot wind at various directions was added to the yawing moment due to the main-rotor torque required to hover out of ground effect. The tail-rotor thrust required to counteract the yawing moment in a 30-knot wind was computed and expressed as a ratio to the thrust required with no wind. These results are presented in figure 17 for the RSRA. The adverse yawing moment of the airframe can increase the thrust required of the tail rotor up to 15 percent.

SUMMARY OF RESULTS

A wind-tunnel investigation has been conducted to determine the contribution of the tail to the aerodynamic characteristics of the rotor systems research aircraft with a tail rotor and without a main rotor. The results can be summarized as follows:

1. Increasing the space between the tail-rotor hub and the vertical tail reduces the tail-rotor torque required at moderate to high rotor thrust.

2. Increasing the exit dynamic pressure of the auxiliary thrust engines decreases the static directional stability.

3. The tail-rotor thrust and its interference provide a positive increment to the static directional stability. The tail contribution to the static directional stability increases with forward speed.

4. The adverse yawing moment of the airframe would strongly affect the thrust required of the tail rotor when the helicopter is hovering in a crosswind.

Langley Research Center
National Aeronautics and Space Administration
Hampton, VA 23665
March 4, 1977

REFERENCES

1. Yeager, William T., Jr.; Young, Warren H., Jr.; and Mantay, Wayne R.: A Wind-Tunnel Investigation of Parameters Affecting Helicopter Directional Control at Low Speeds in Ground Effect. NASA TN D-7694, 1974.

2. Mineck, Raymond E.; and Freeman, Carl E.: Aerodynamic Characteristics of a 1/6-Scale Powered Model of the Rotor Systems Research Aircraft. NASA TM X-3489, 1977.

3. Linden, A. W.; and Hellyar, M. W.: The Rotor Systems Research Aircraft - A Flying Wind Tunnel. AIAA Paper No. 74-1277, Oct. 1974.

4. Mechtly, E. A.: The International System of Units - Physical Constants and Conversion Factors (Second Revision). NASA SP-7012, 1973.

5. Mineck, Raymond E.; Freeman, Carl E.; and Hassell, James L., Jr.: Aerodynamic Characteristics of a 1/6-Scale Model of the Rotor Systems Research Aircraft With the Rotors Removed. NASA TN D-8198, 1976.

6. Horst, Terri J.; and Reschak, Robert J.: Designing To Survive Tail Rotor Loss. American Helicopter Soc. Preprint No. 942, May 1975.

7. Wilson, John C.; and Mineck, Raymond E.: Wind-Tunnel Investigation of Helicopter-Rotor Wake Effects on Three Helicopter Fuselage Models. NASA TM X-3185, 1975.

TABLE I.- MODEL DATA

Tail rotor:	
Number of blades	4
Airfoil section	NACA 0012
Radius, m (ft)	0.269 (0.883)
Blade chord, m (ft)	0.051 (0.167)
Blade twist, deg	-4
Solidity	0.240
Area, m^2 (ft^2)	0.228 (2.450)
Hinge offset, m (ft)	0.019 (0.062)
Pitch-flap coupling, deg	-45
Lock number	3.5
Vertical tail:	
Airfoil section	NACA 0015
Reference area, m^2 (ft^2)	0.214 (2.287)
Span, cm (in.)	64.01 (25.20)
Mean aerodynamic chord, cm (in.)	35.36 (13.92)
Aspect ratio	1.93
Taper ratio	0.37

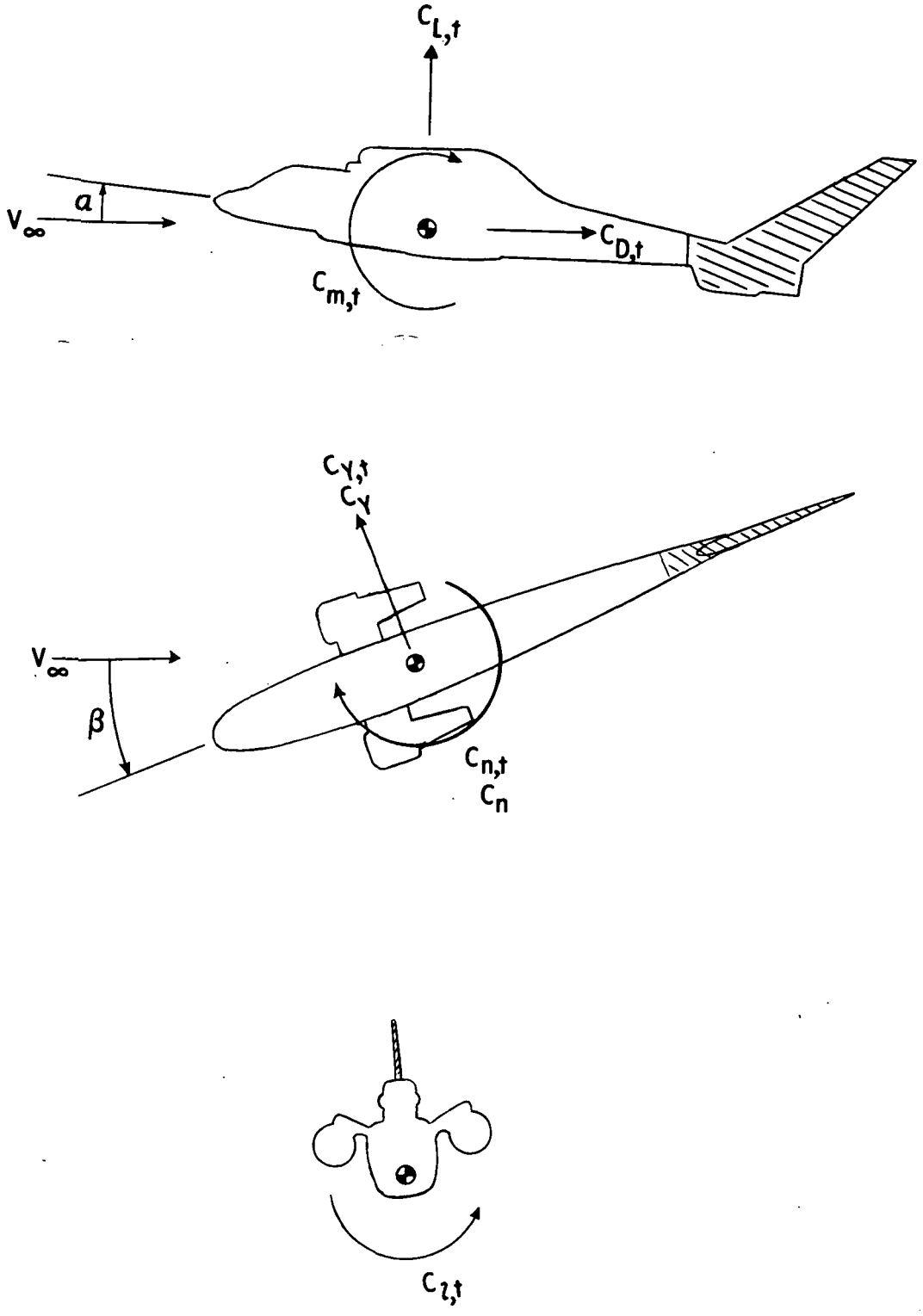

(a) Airframe and tail assembly. (Tail assembly hatched.)

Figure 1.- Sign conventions for forces, moments, and angles.

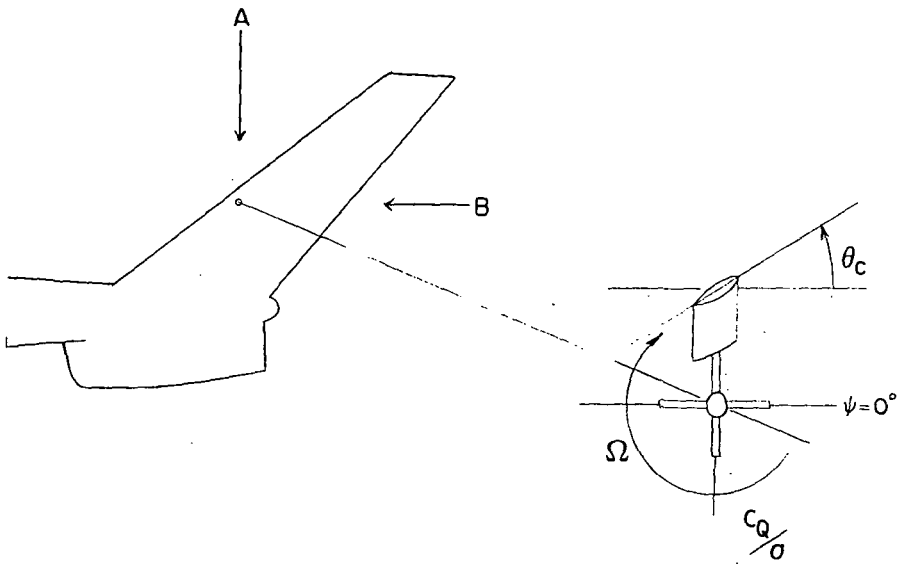

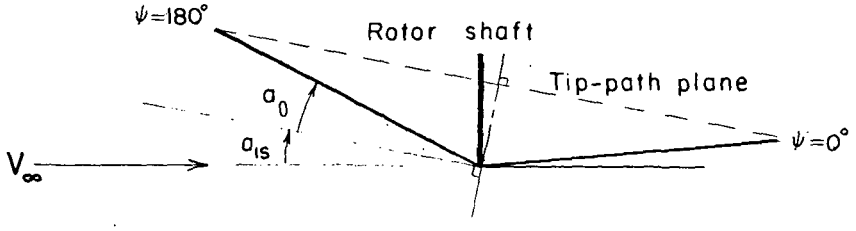

View from above (A)

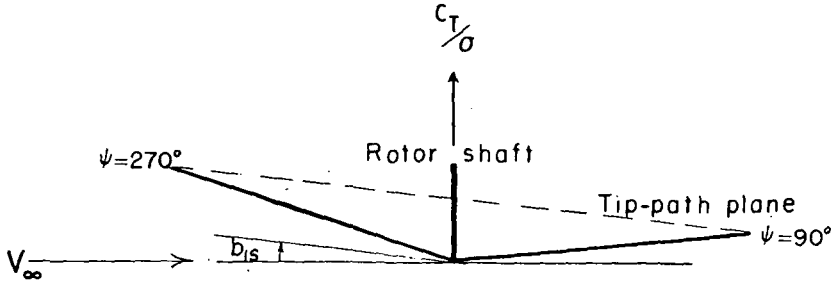

View from rear (B)

(b) Tail rotor.

Figure 1.- Concluded.

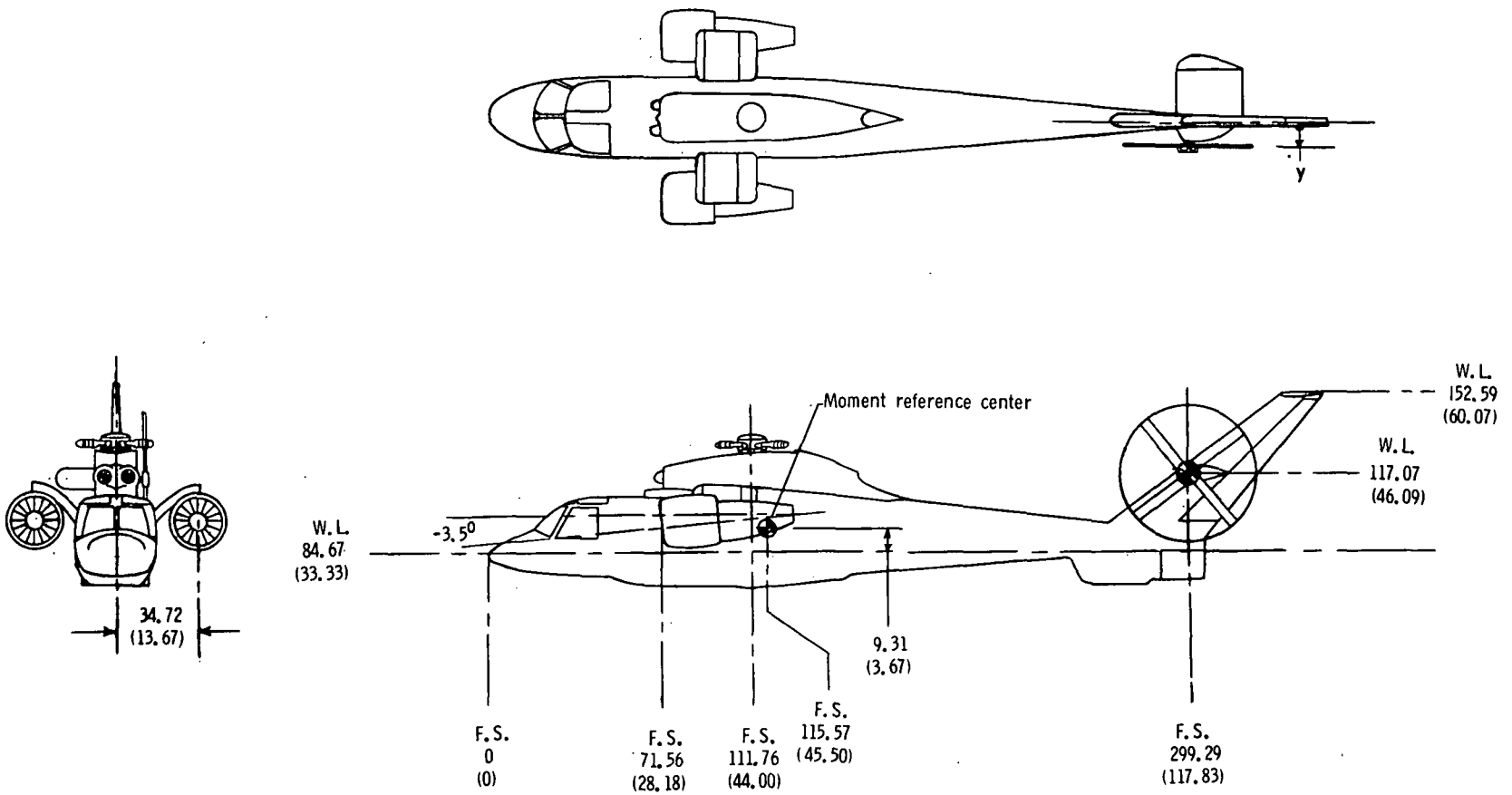

(a) Three-view sketch.

Figure 2.- Details of model. All dimensions are in cm (in.) unless otherwise specified.

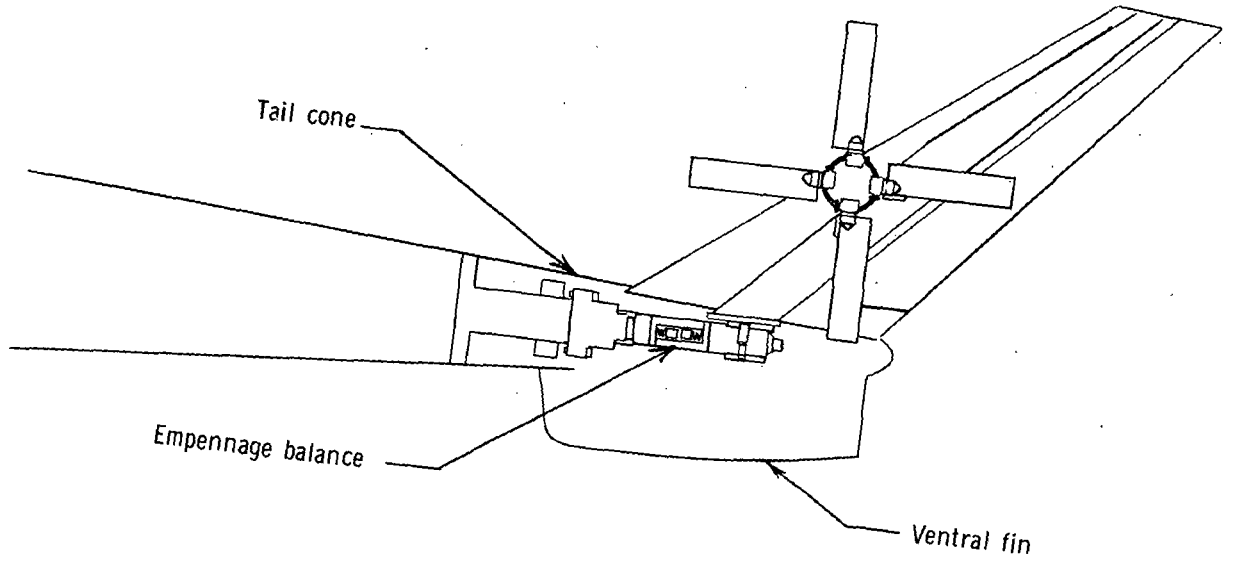

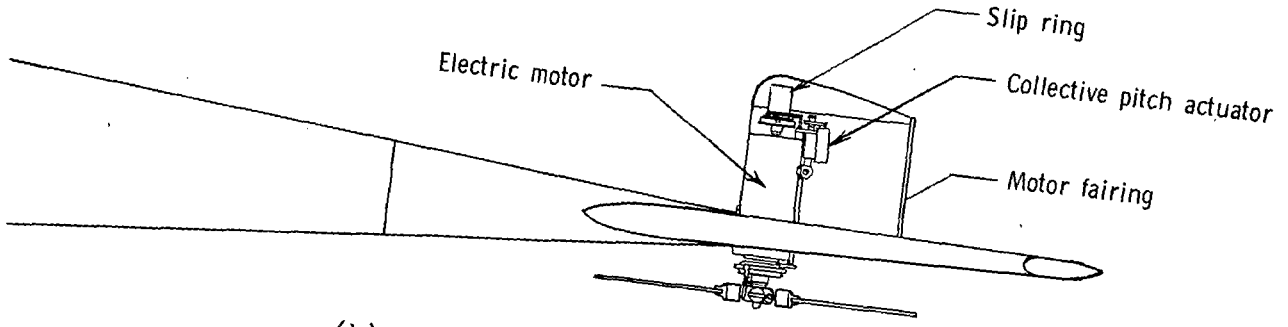

(b) Internal layout of empennage.

Figure 2.- Continued.

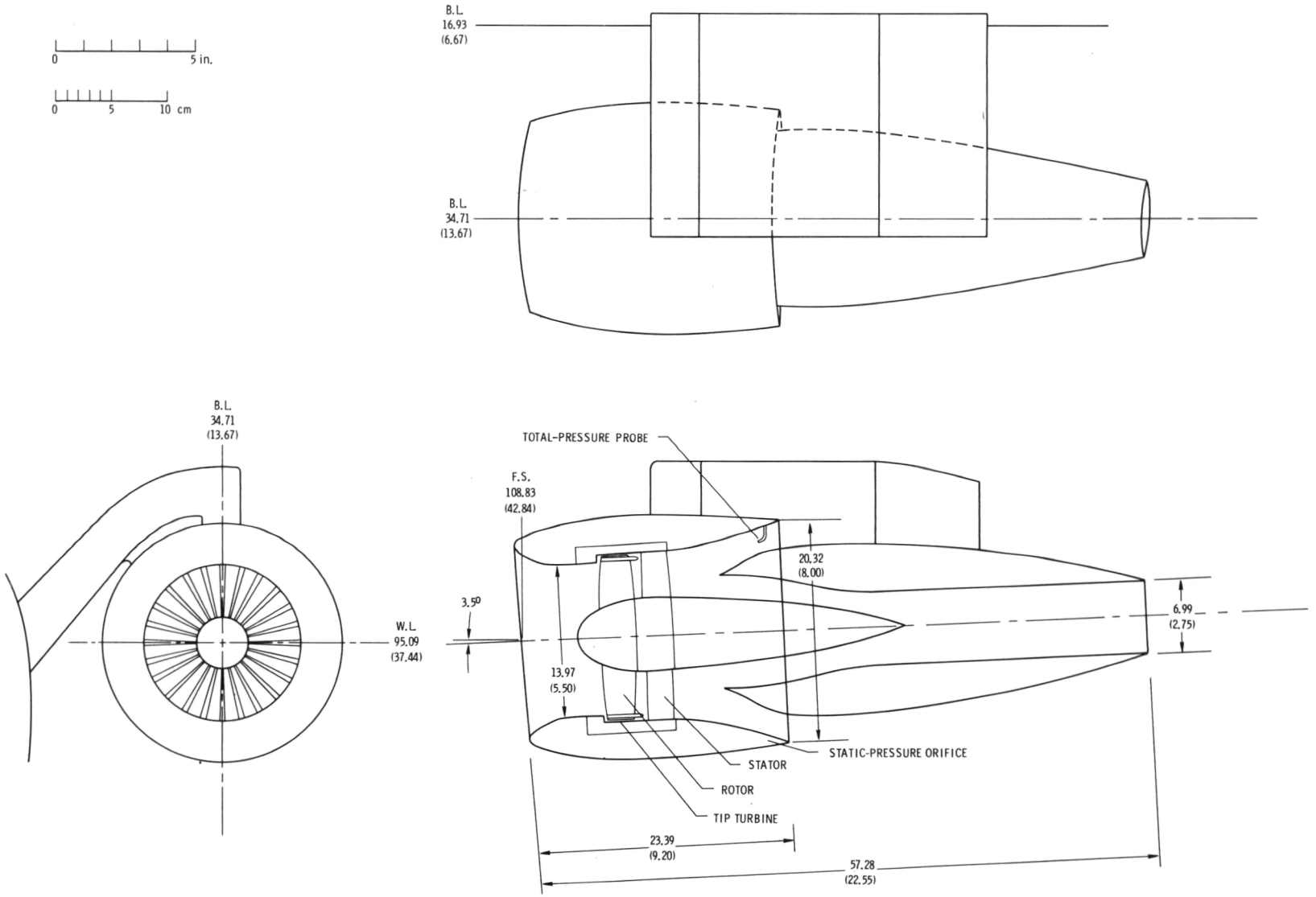

(c) Three-view sketch of auxiliary thrust engine simulators.

Figure 2.- Concluded.

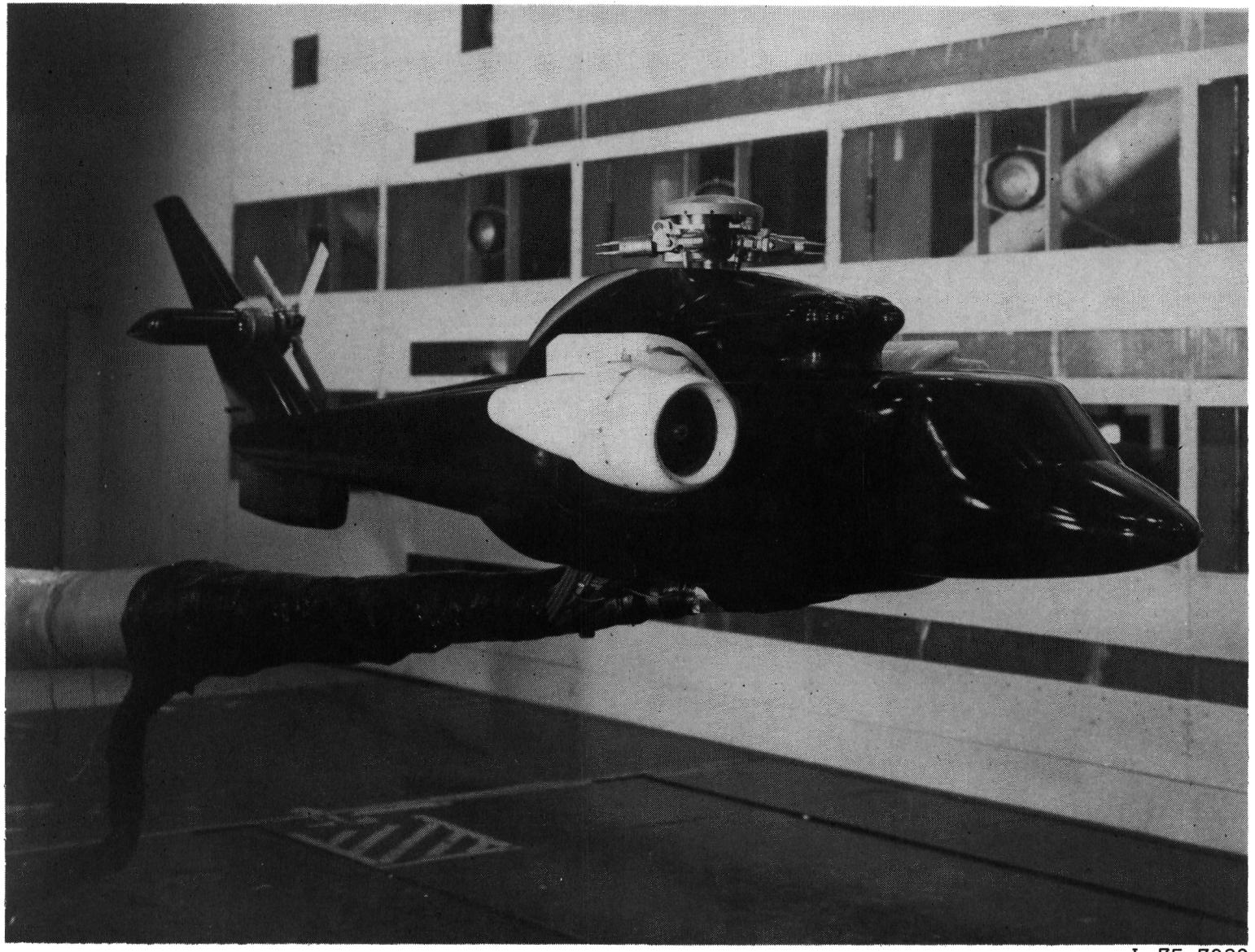

L-75-7930

(a) Three-quarter front view.

Figure 3.- Model in Langley V/STOL tunnel.

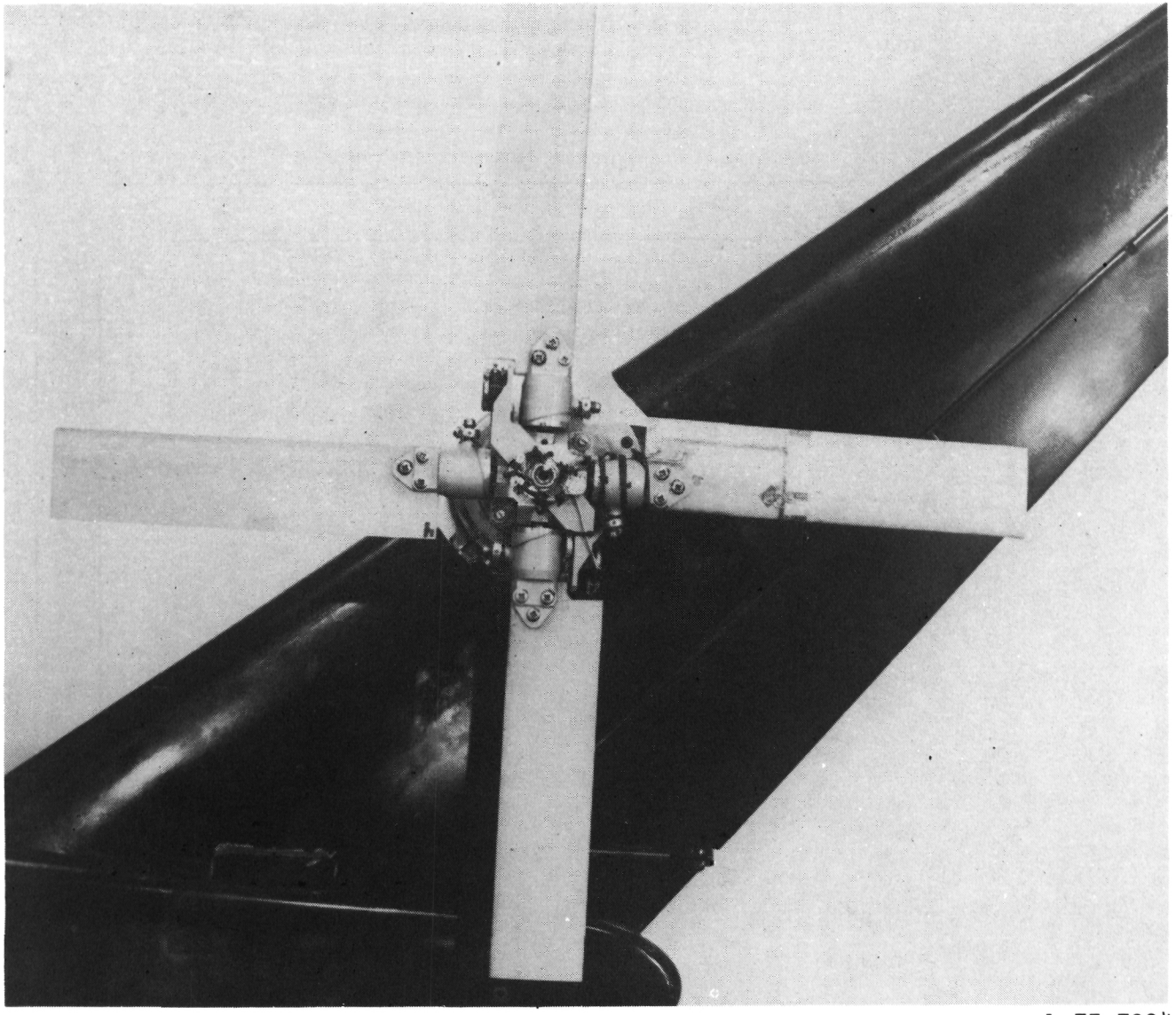

L-75-7904

(b) Tail rotor and empennage.

Figure 3.- Concluded.

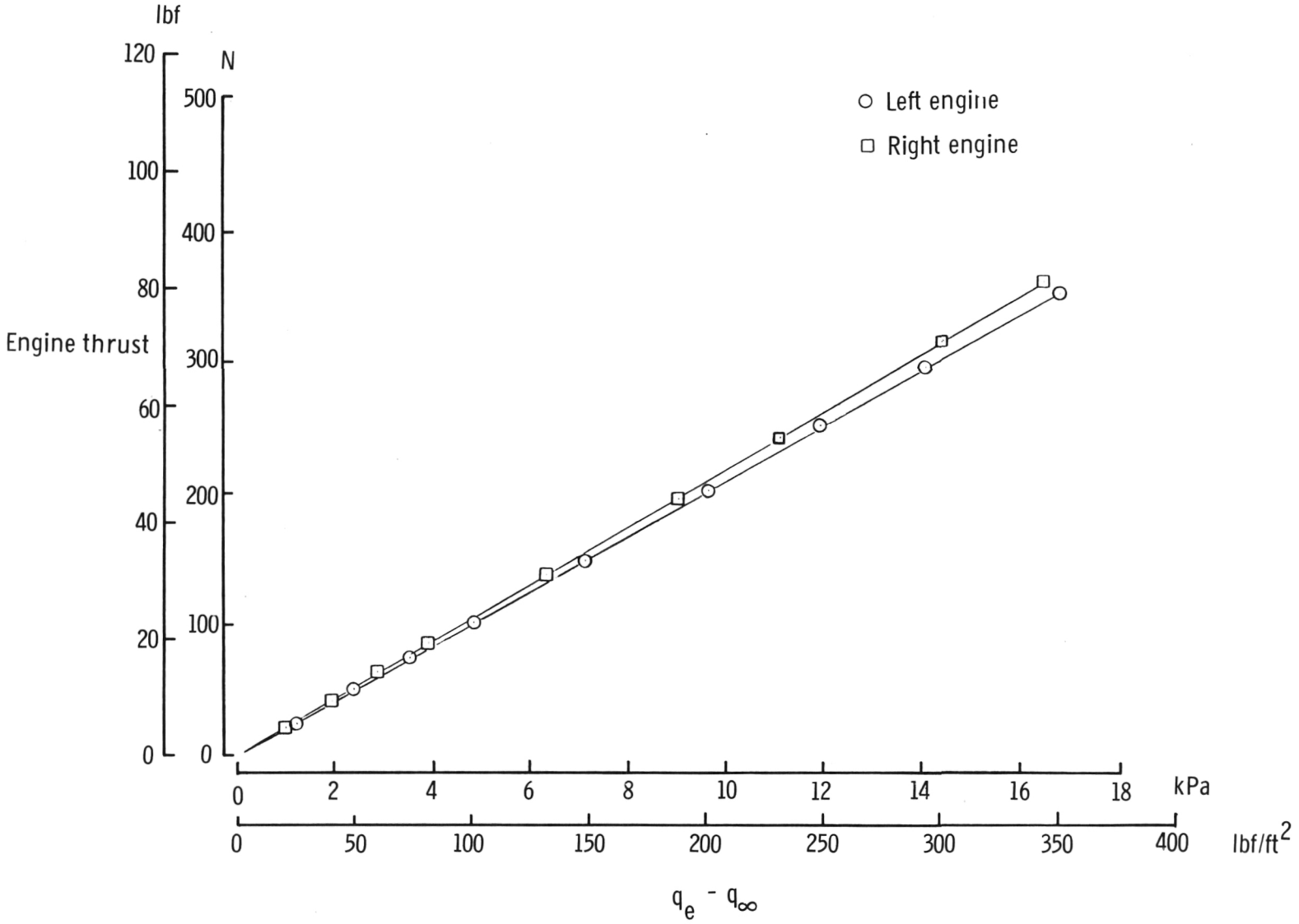

Figure 4.- Calibrated auxiliary engine thrust.

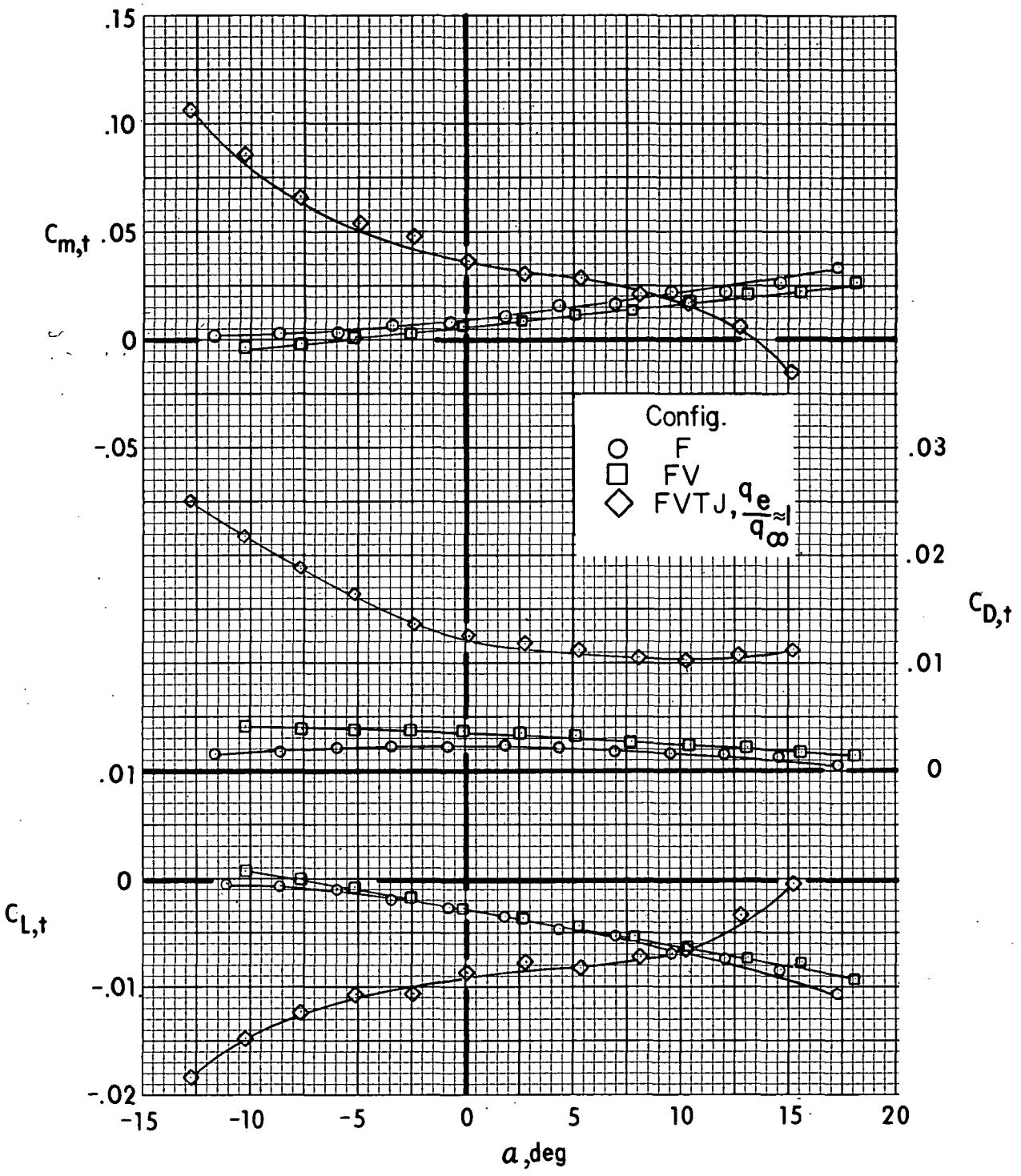

Figure 5.- Effect of tail components on longitudinal aerodynamic characteristics of tail assembly without tail rotor.

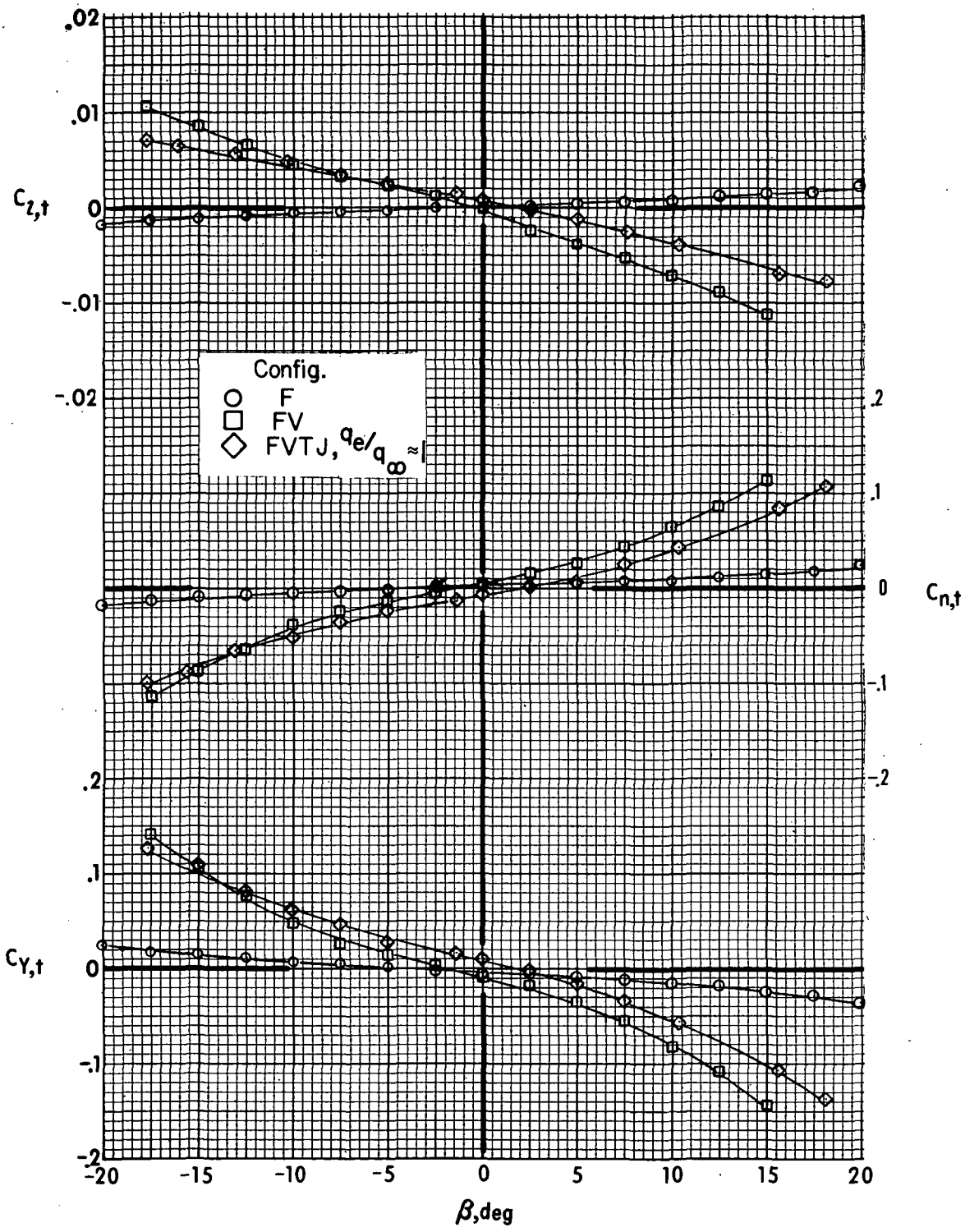

Figure 6.- Effect of tail components on lateral aerodynamic characteristics of tail assembly without tail rotor. $\alpha = 0^{\circ}$.

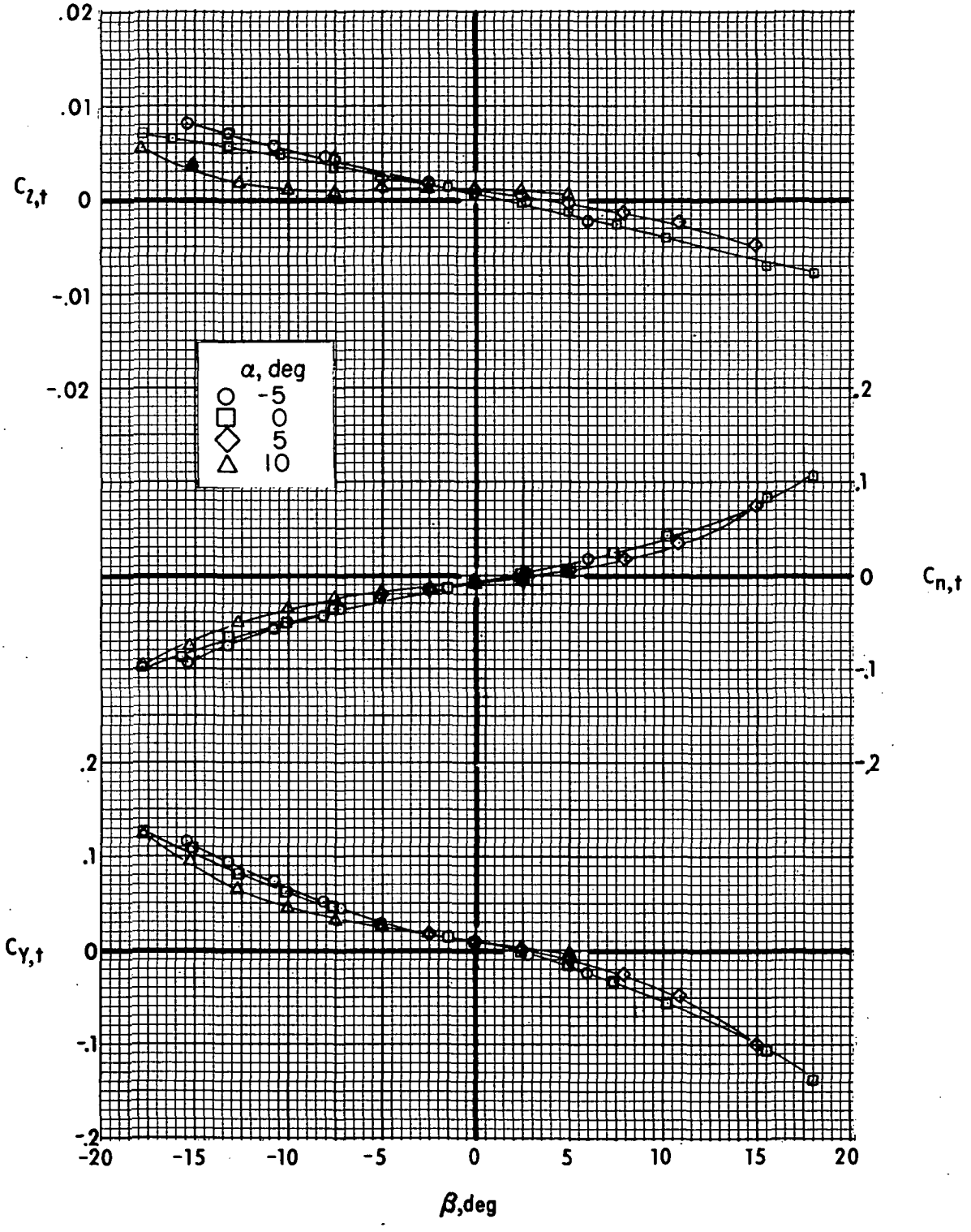

Figure 7.- Effect of angle of attack on lateral aerodynamic characteristics of tail assembly without tail rotor. FVTJ; $q_e/q_\infty \approx 1$.

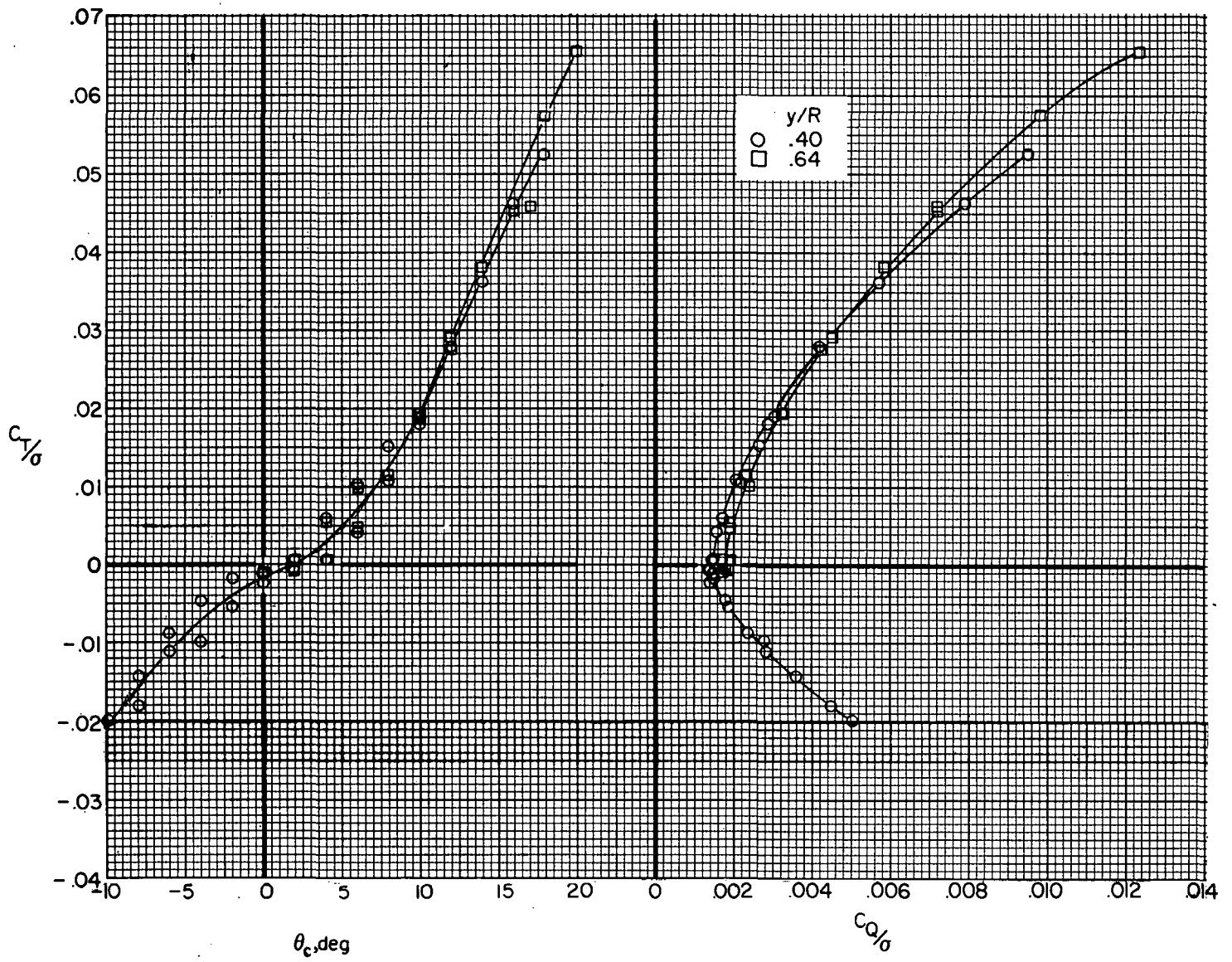

(a) C_T/σ and C_Q/σ.

Figure 8.- Effect of lateral hub spacing on tail-rotor aerodynamic characteristics. $\mu = 0$.

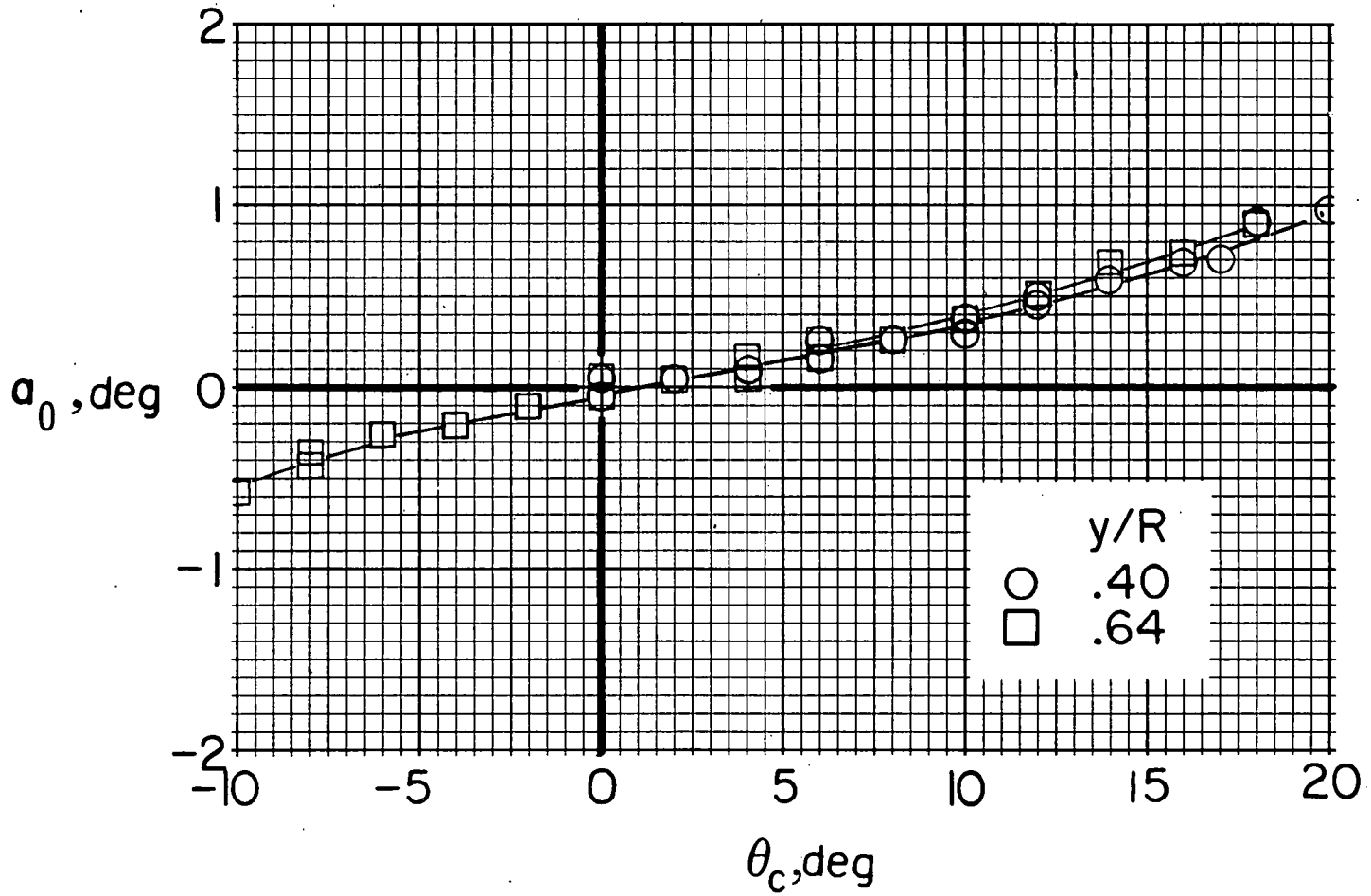

(b) a_0.

Figure 8.- Concluded.

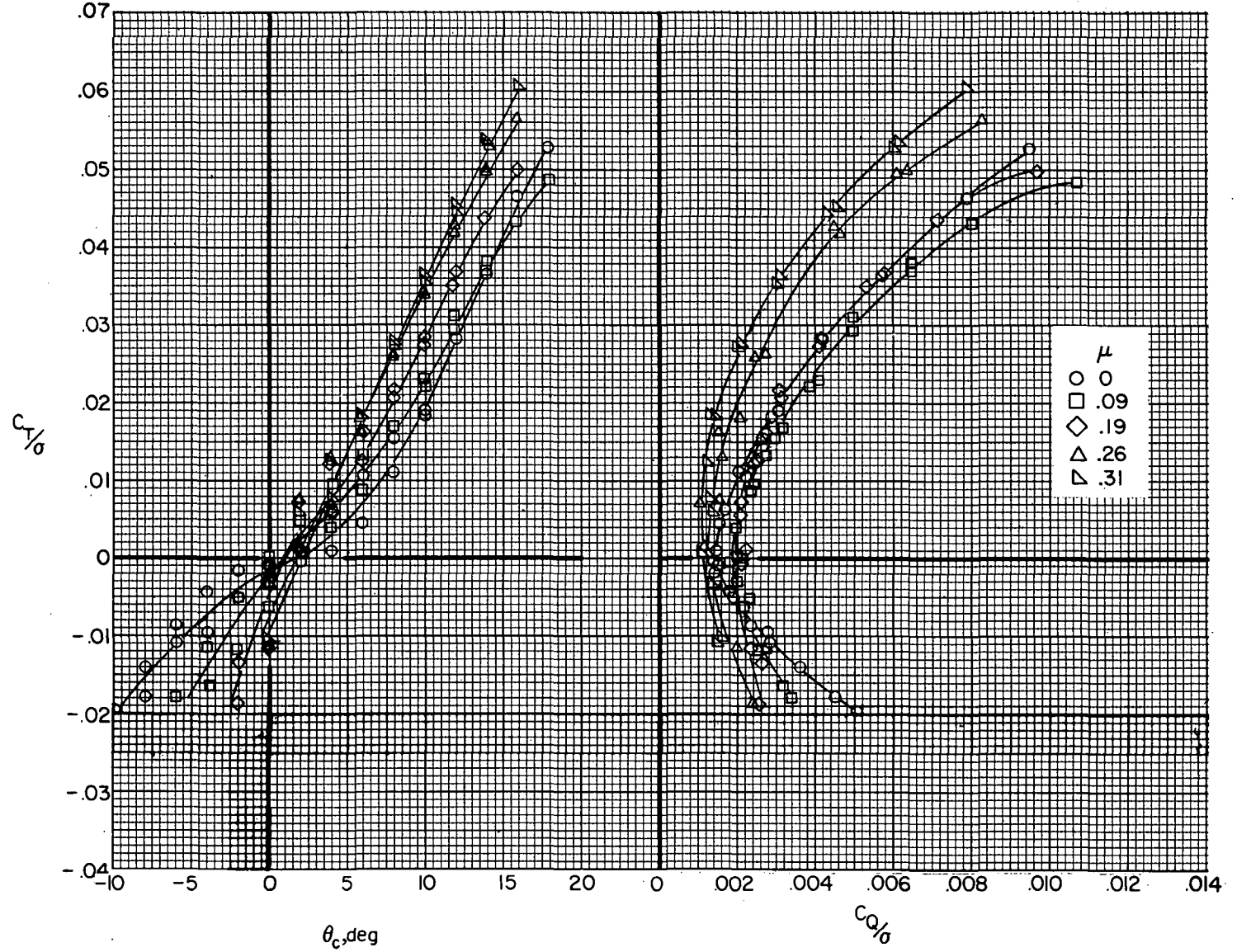

(a) C_T/σ and C_Q/σ.

Figure 9.- Effect of advance ratio on tail-rotor aerodynamic characteristics. $\alpha = -10^\circ$.

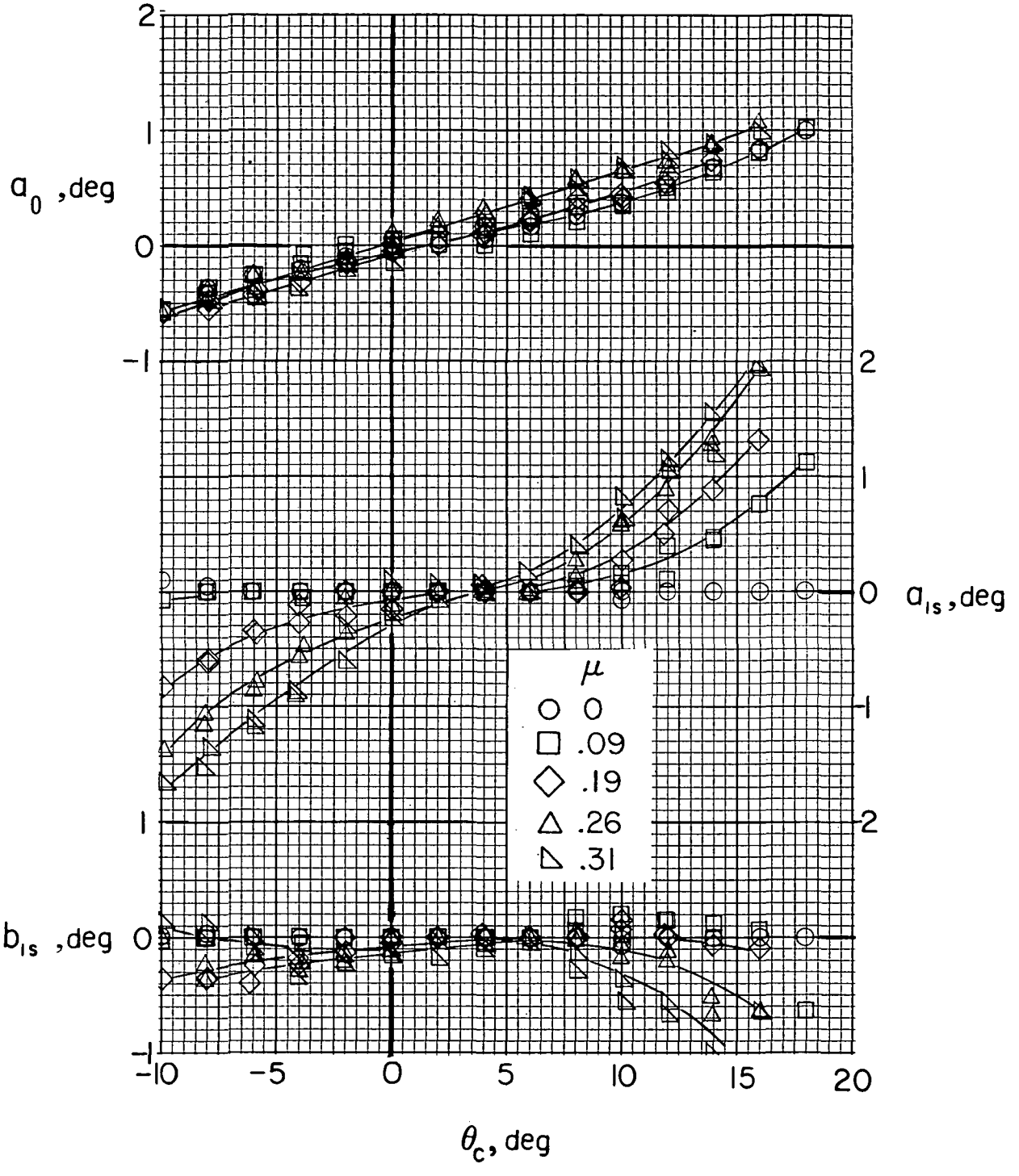

(b) a_0, a_{1s}, and b_{1s}.

Figure 9.- Concluded.

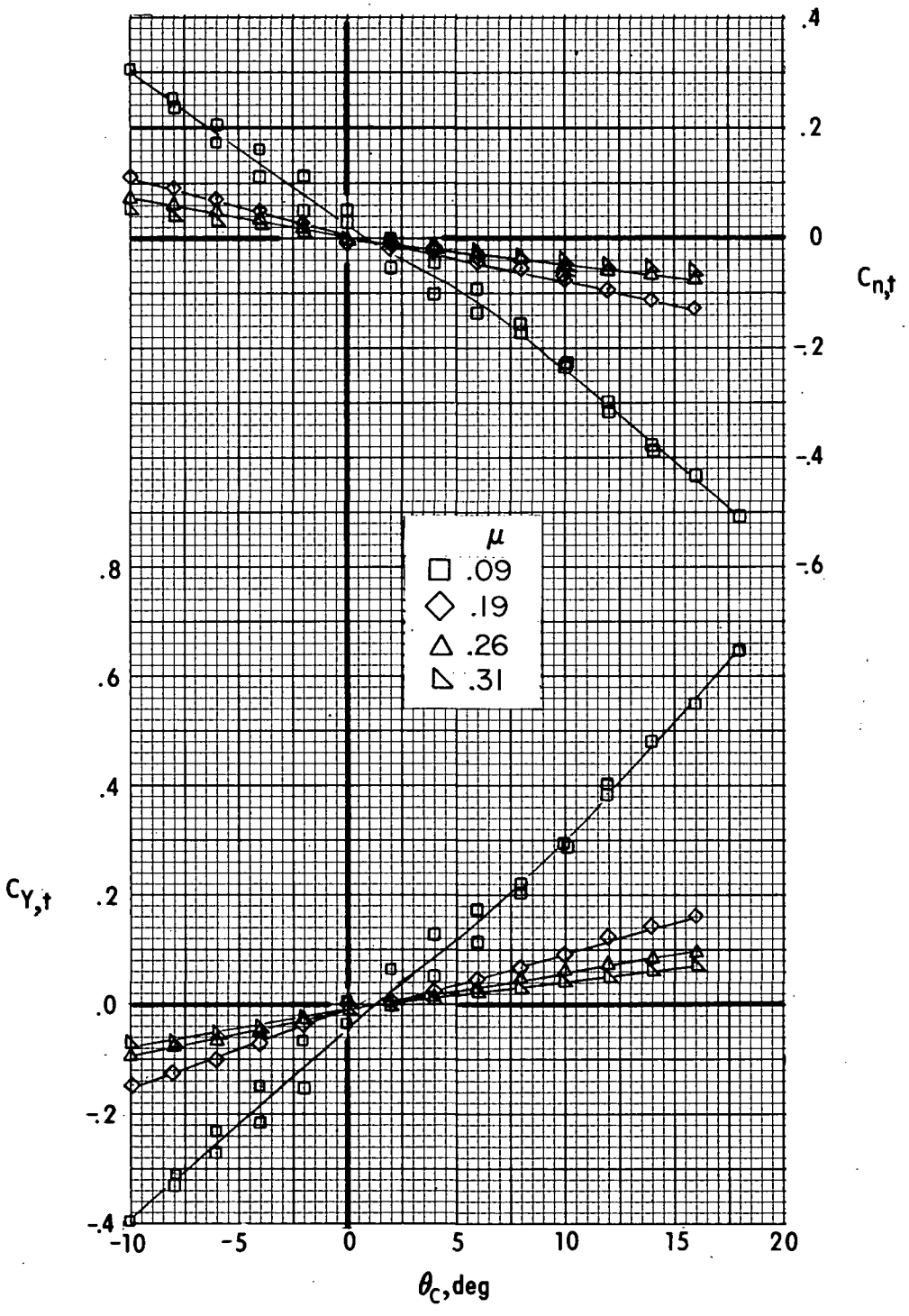

Figure 10.- Variation of tail aerodynamic characteristics with tail-rotor collective pitch for several forward speeds. $\alpha = -10^{o}$.

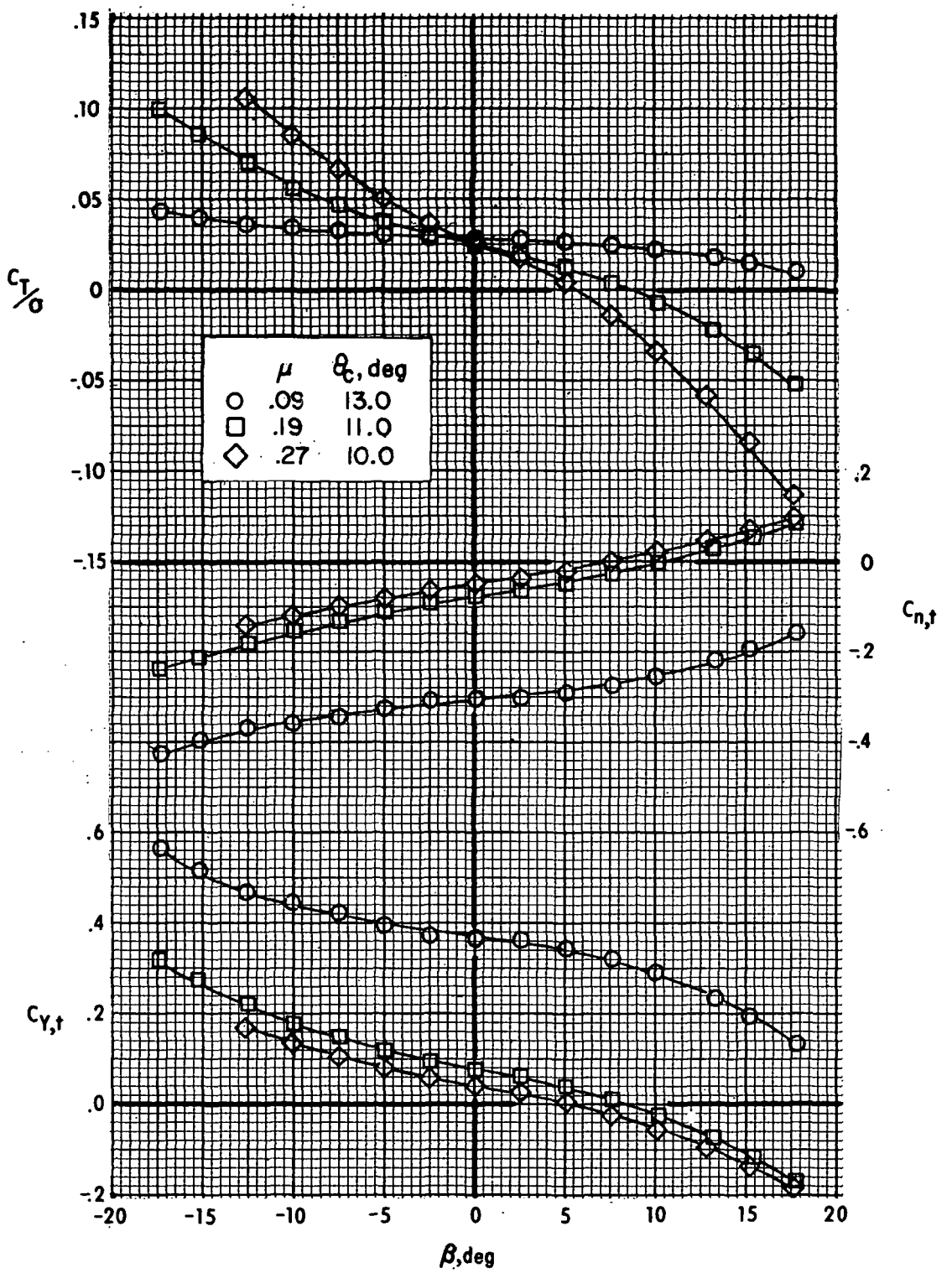

(a) No auxiliary engine thrust. $q_e/q_\infty \approx 1.0$.

Figure 11.- Effect of forward speed on aerodynamic characteristics of tail. $\alpha = 0^o$.

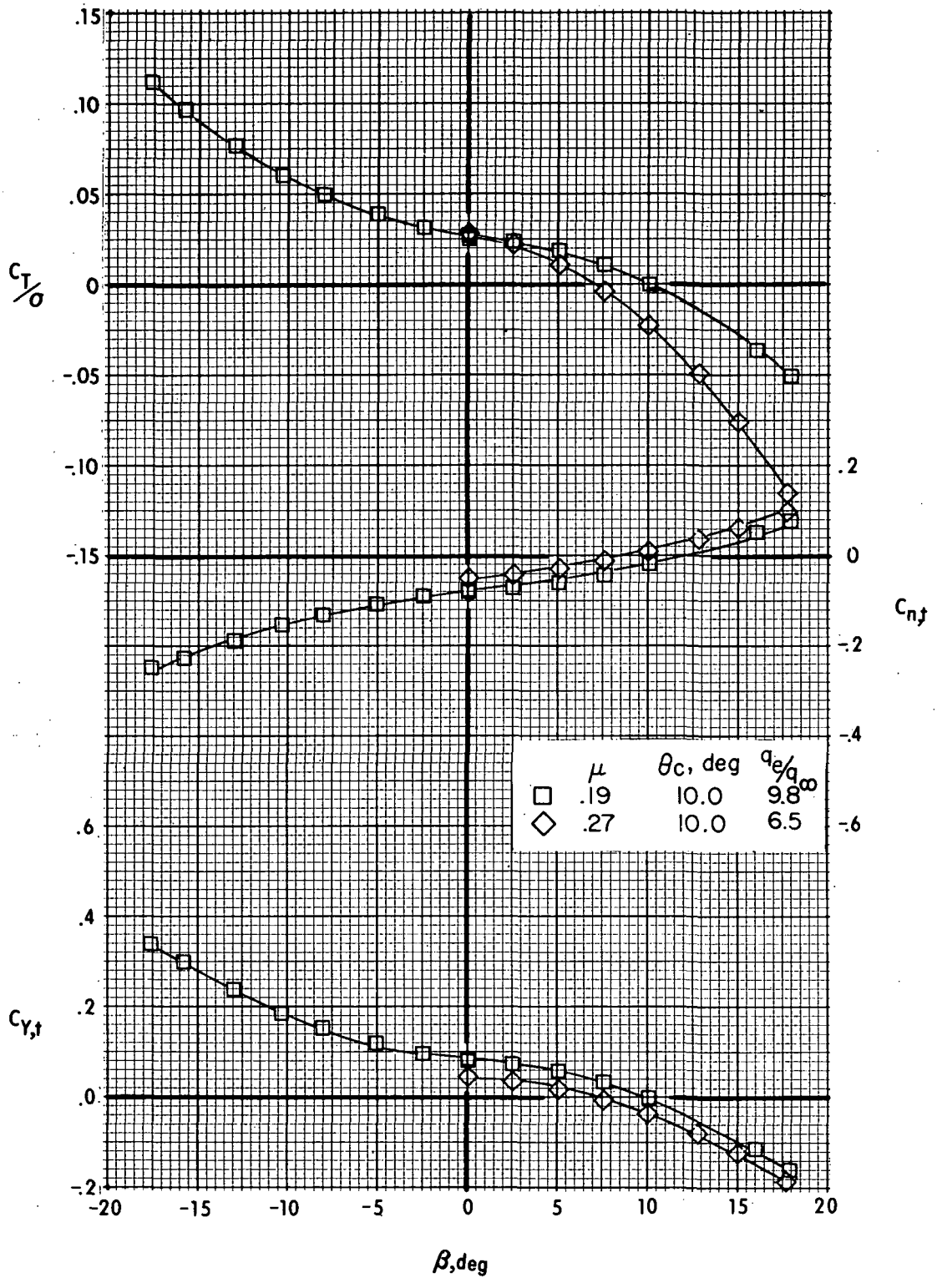

(b) With auxiliary engine thrust. $q_e/q_\infty > 1.0$.

Figure 11.- Concluded.

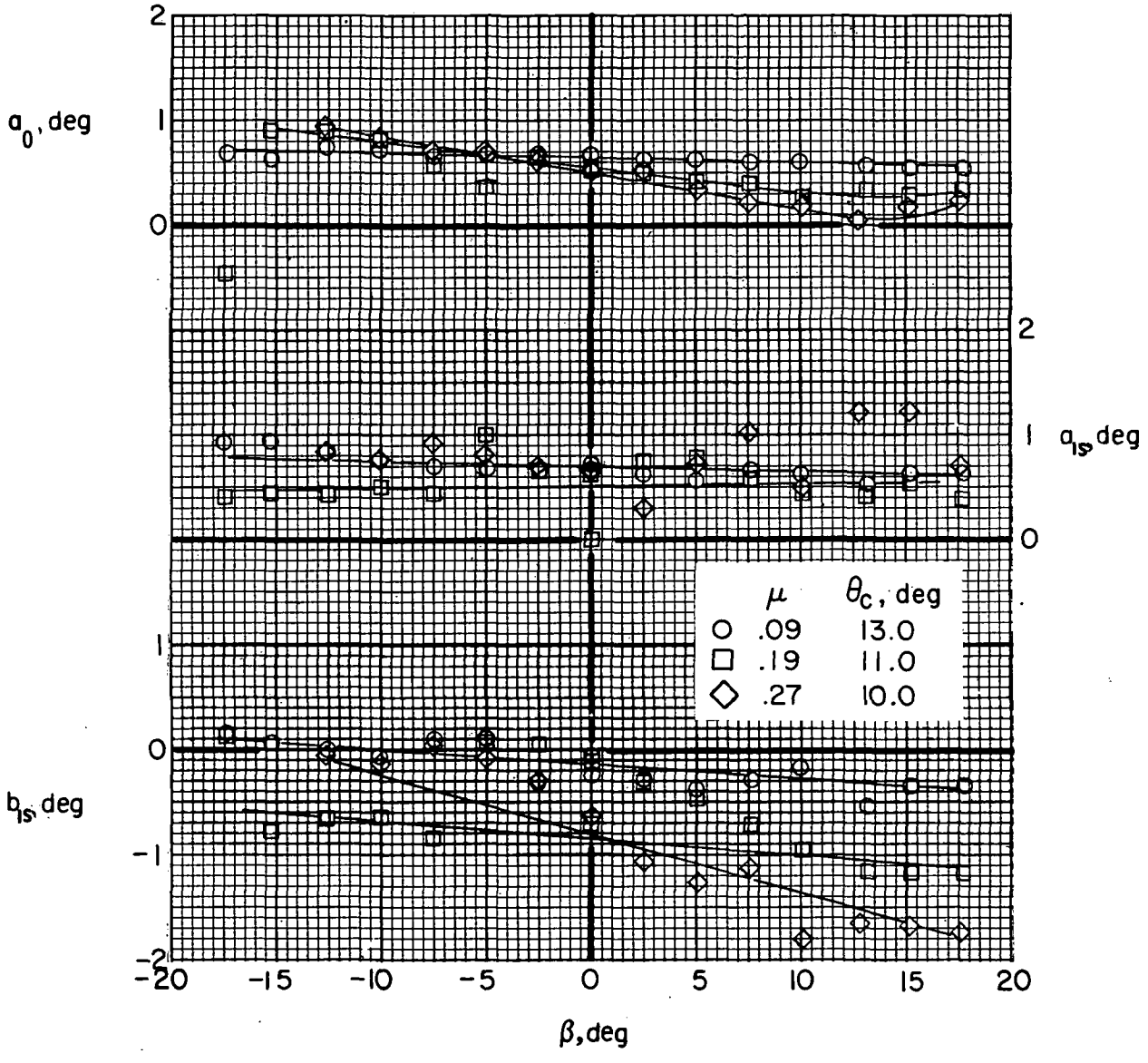

(a) No auxiliary engine thrust. $q_e/q_\infty \approx 1.0$.

Figure 12.- Effect of forward speed on tail-rotor flapping. $\alpha \approx 0^o$.

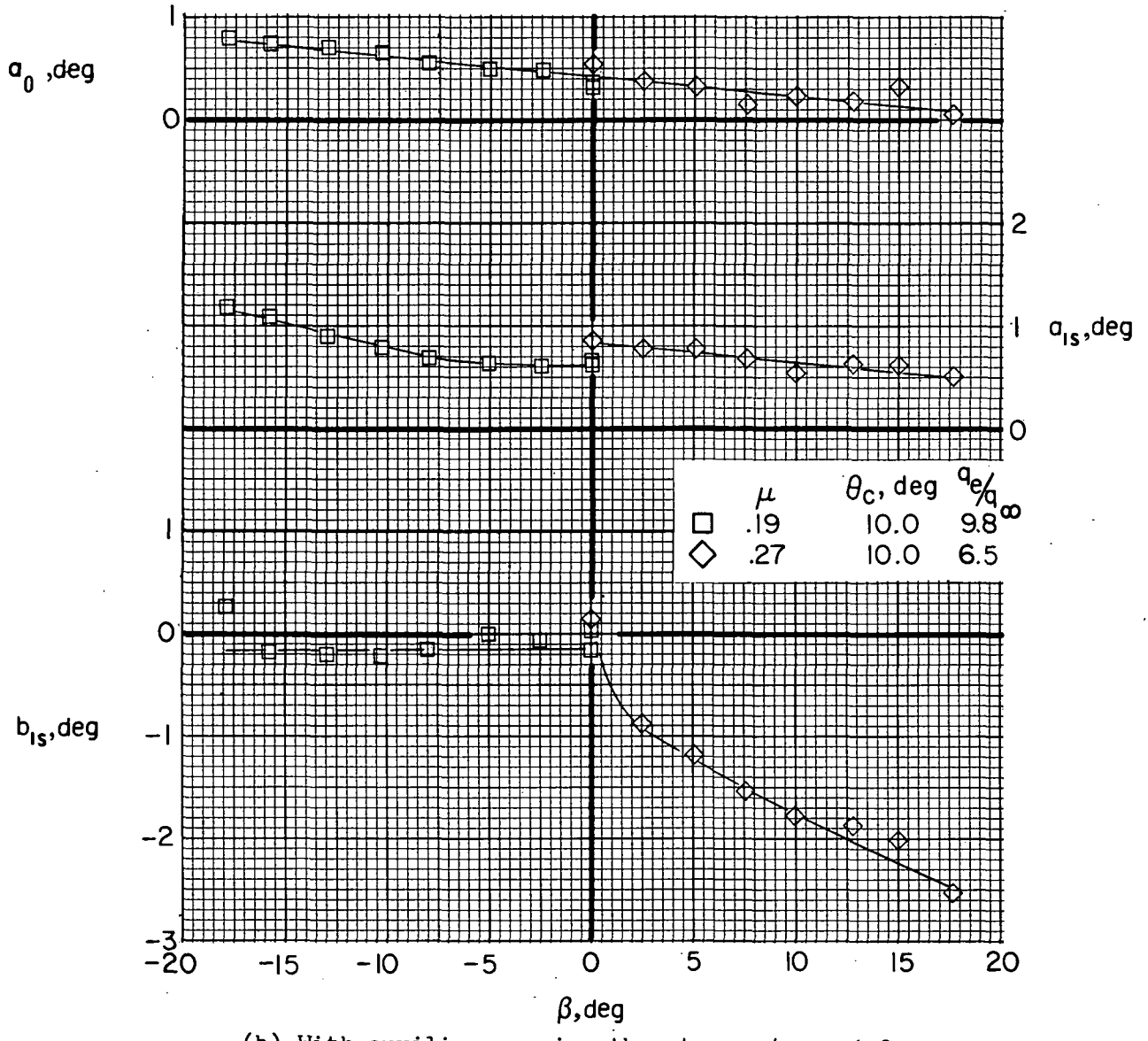

(b) With auxiliary engine thrust. $q_e/q_\infty > 1.0$.

Figure 12.- Concluded.

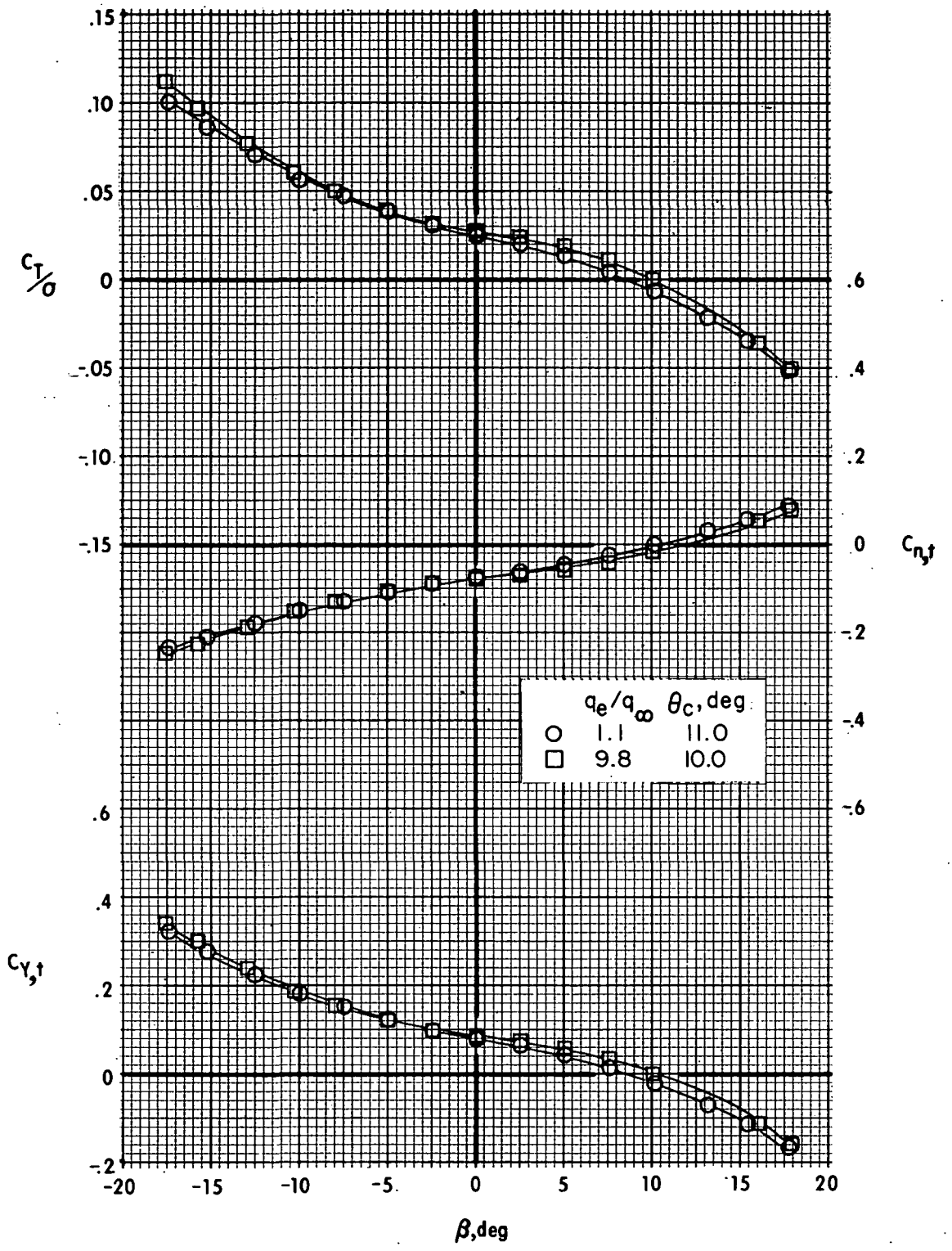

(a) $\mu \approx 0.19$.

Figure 13.- Effect of auxiliary engine thrust on tail aerodynamic characteristics. $\alpha \approx 0^o$.

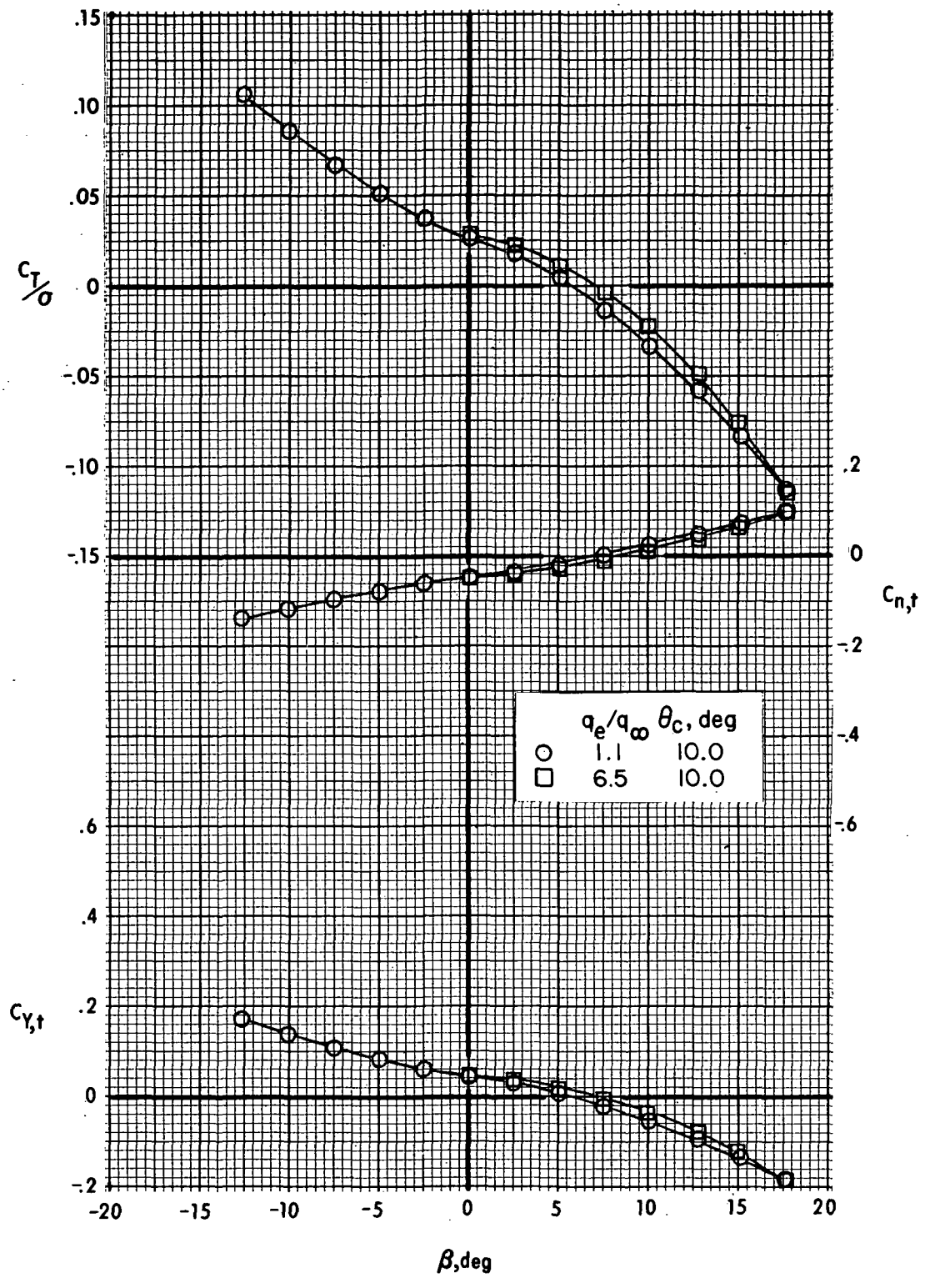

(b) $\mu = 0.27$.

Figure 13.- Concluded.

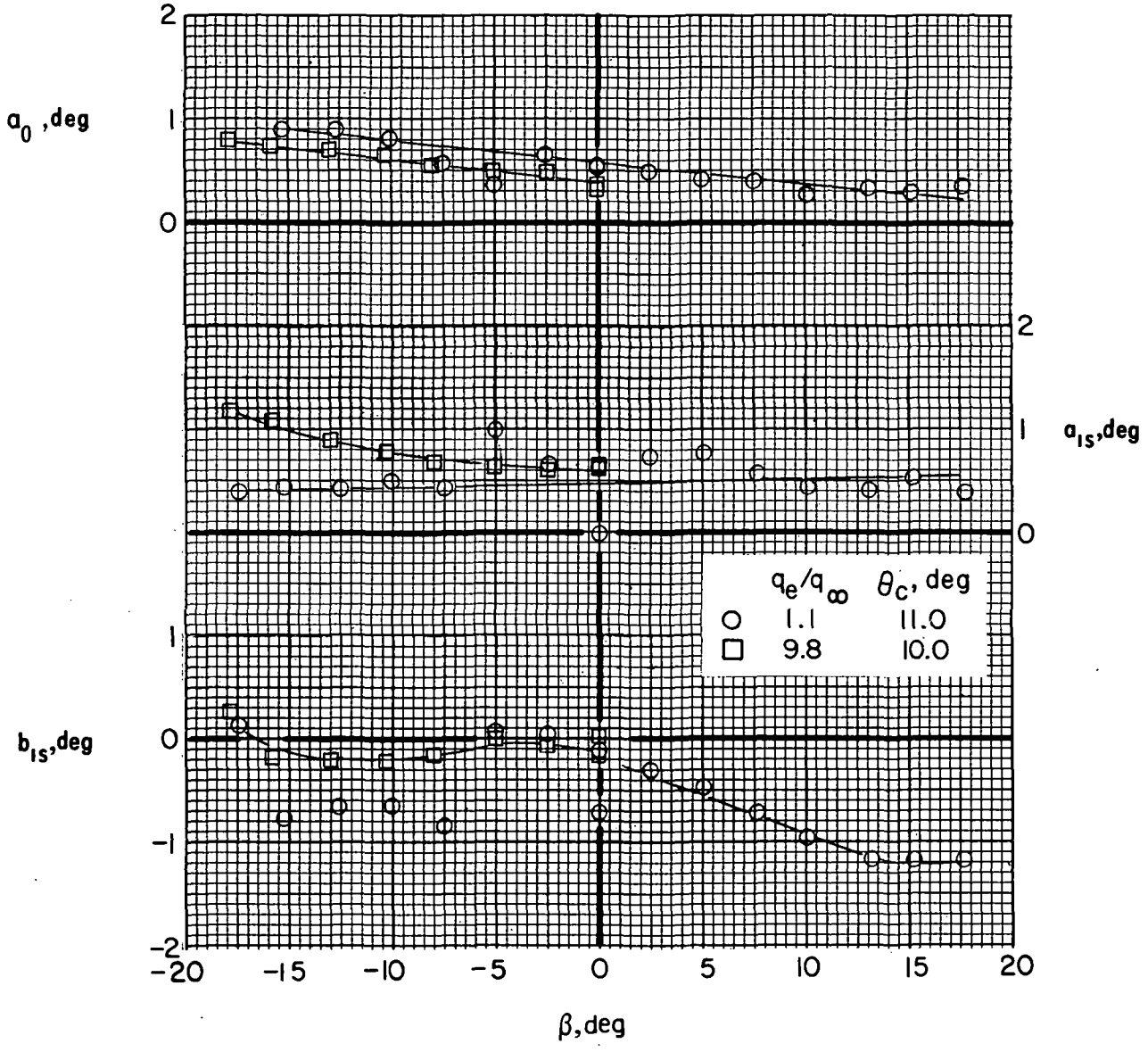

(a) $\mu \approx 0.19$.

Figure 14.- Effect of auxiliary engine thrust on tail-rotor flapping. $\alpha \approx 0^o$.

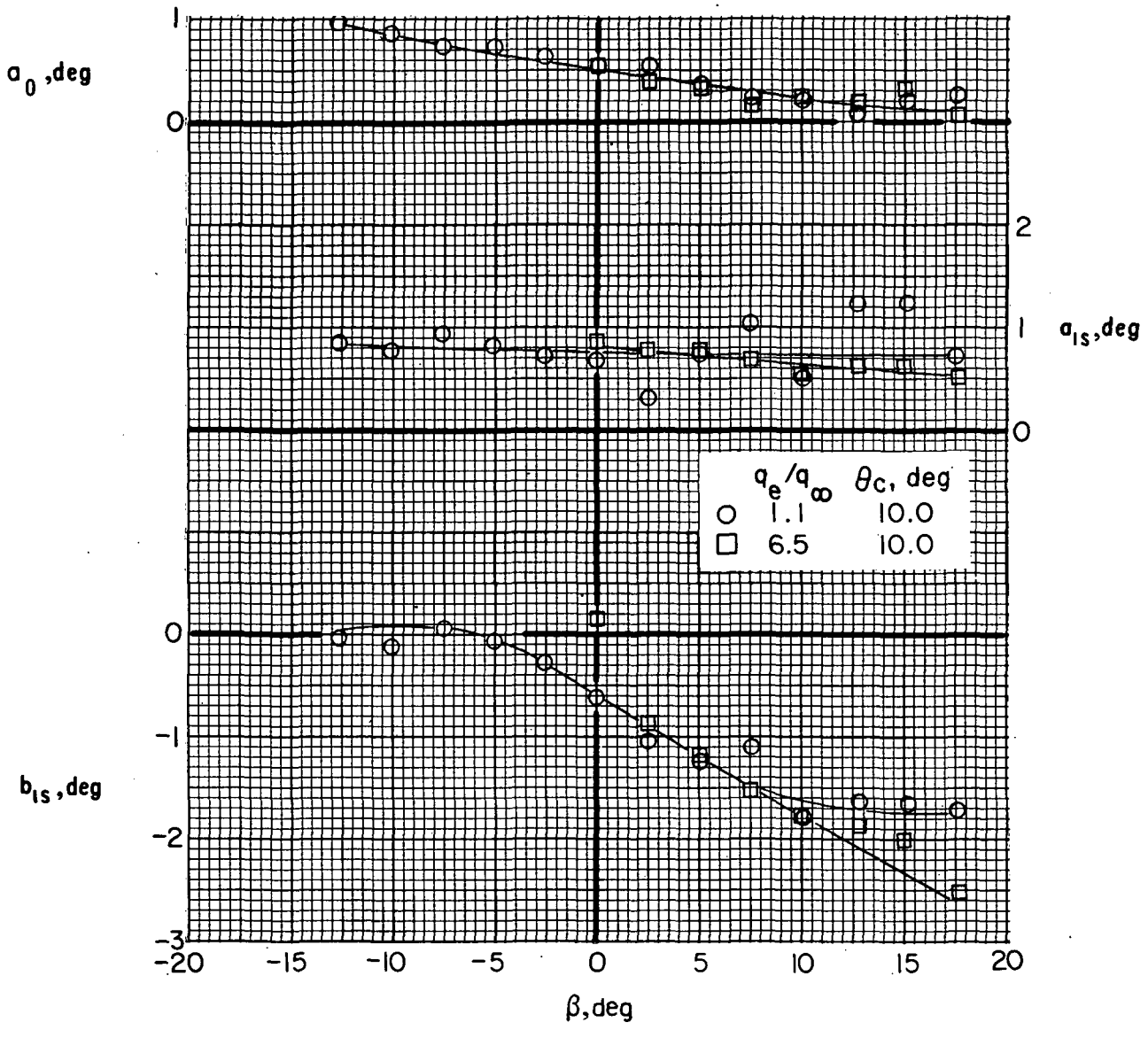

(b) $\mu \approx 0.27$.

Figure 14.- Concluded.

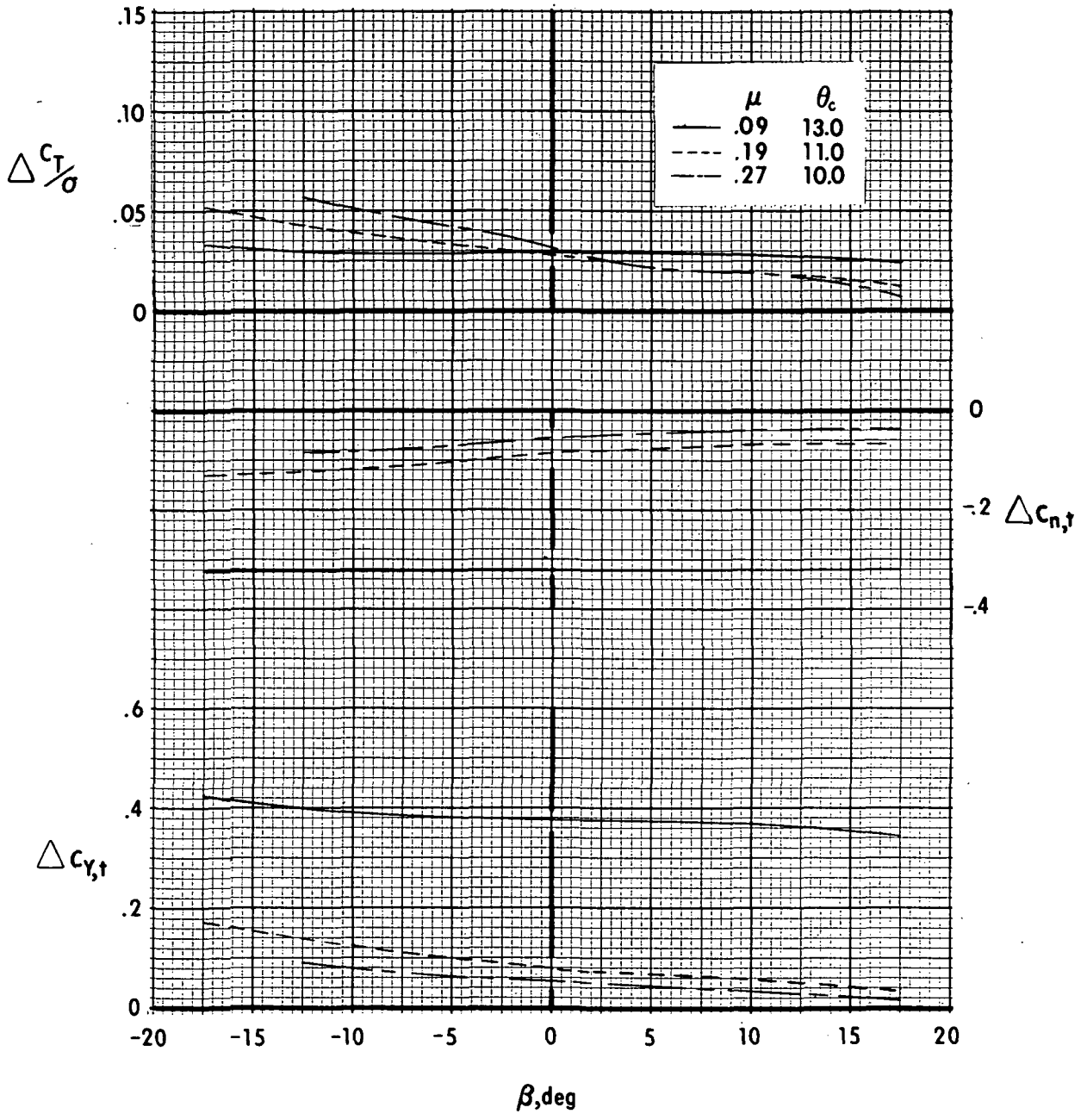

Figure 15.- Effect of forward speed on aerodynamic characteristics with vertical tail-assembly loads removed. $q_e/q_\infty = 1.0$; $\alpha = 0^o$.

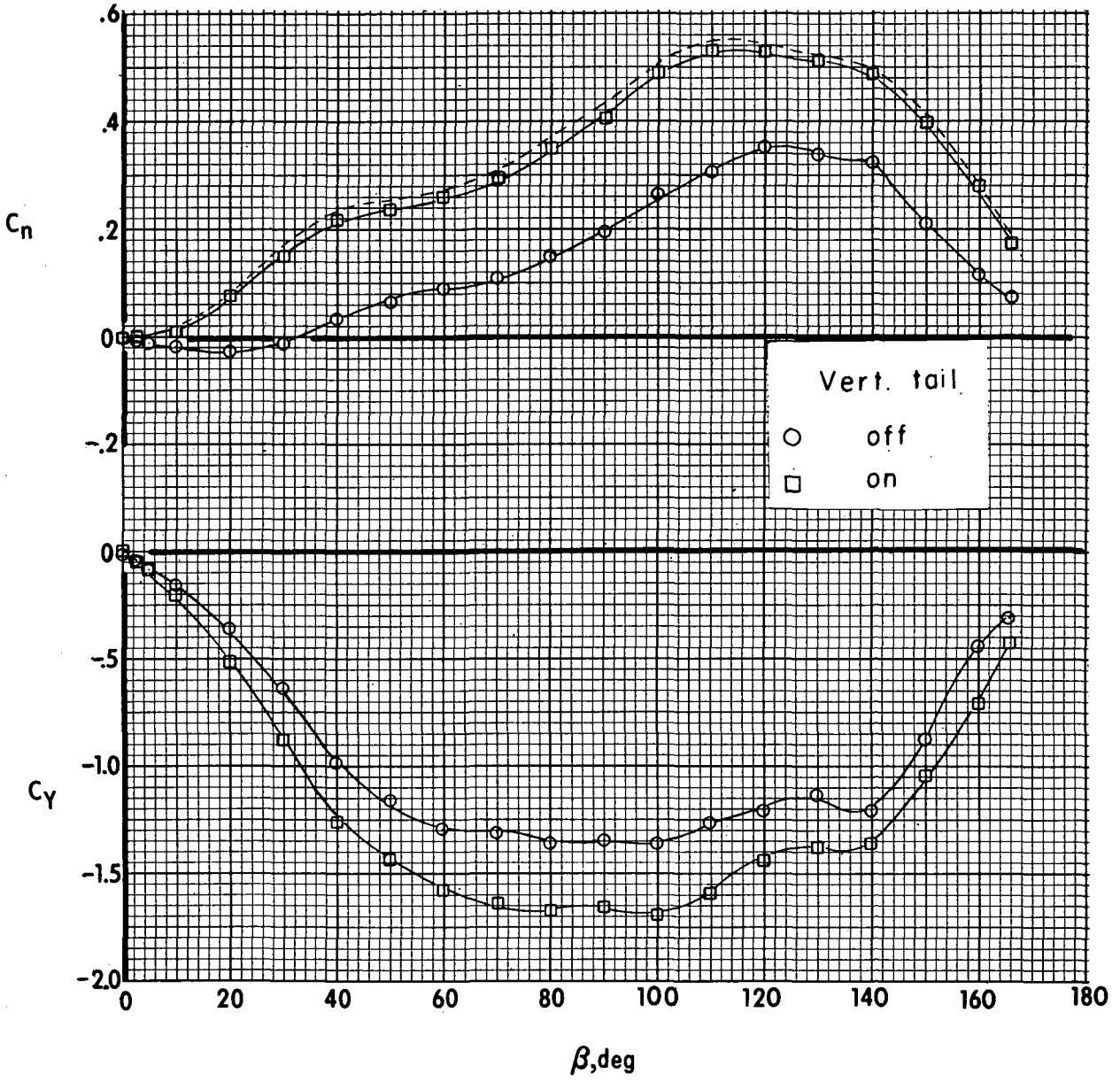

Figure 16.- Effect of tail components on airframe aerodynamic characteristics without tail rotor. $\alpha \approx 0^{o}$. (Data shown are for reduced-span vertical tail (ref. 5). Extrapolated results for full-span vertical tail are shown as a dashed line.)

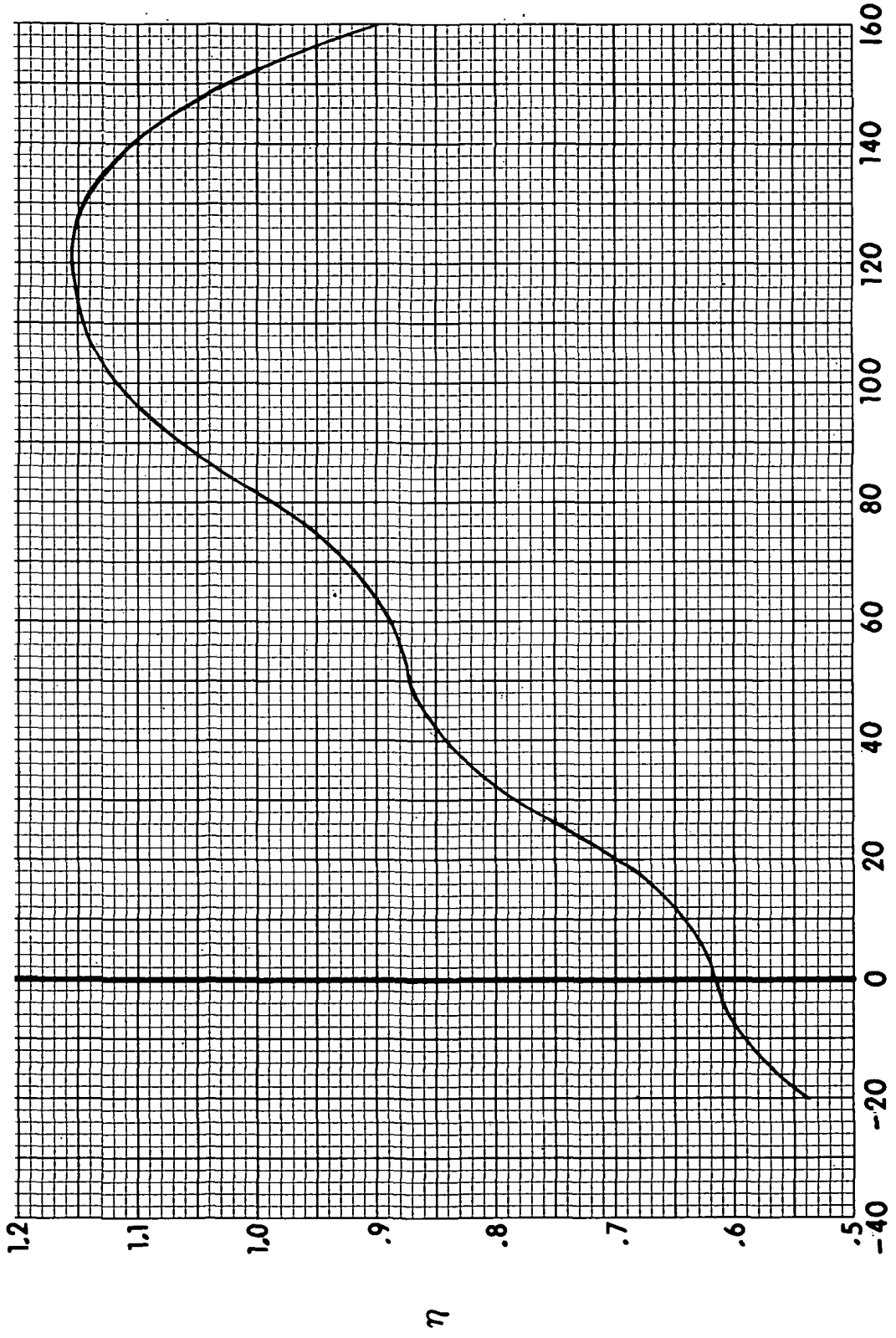

Figure 17.- Tail-rotor thrust required for the RSRA helicopter configuration to hover in a 30-knot wind.

NATIONAL AERONAUTICS AND SPACE ADMINISTRATION
WASHINGTON, D.C. 20546

OFFICIAL BUSINESS
PENALTY FOR PRIVATE USE $300

SPECIAL FOURTH-CLASS RATE
BOOK

POSTAGE AND FEES PAID
NATIONAL AERONAUTICS AND
SPACE ADMINISTRATION
451

U.S.MAIL

POSTMASTER: If Undeliverable (Section 158 Postal Manual) Do Not Return

"The aeronautical and space activities of the United States shall be conducted so as to contribute . . . to the expansion of human knowledge of phenomena in the atmosphere and space. The Administration shall provide for the widest practicable and appropriate dissemination of information concerning its activities and the results thereof."

—NATIONAL AERONAUTICS AND SPACE ACT OF 1958

NASA SCIENTIFIC AND TECHNICAL PUBLICATIONS

TECHNICAL REPORTS: Scientific and technical information considered important, complete, and a lasting contribution to existing knowledge.

TECHNICAL NOTES: Information less broad in scope but nevertheless of importance as a contribution to existing knowledge.

TECHNICAL MEMORANDUMS: Information receiving limited distribution because of preliminary data, security classification, or other reasons. Also includes conference proceedings with either limited or unlimited distribution.

CONTRACTOR REPORTS: Scientific and technical information generated under a NASA contract or grant and considered an important contribution to existing knowledge.

TECHNICAL TRANSLATIONS: Information published in a foreign language considered to merit NASA distribution in English.

SPECIAL PUBLICATIONS: Information derived from or of value to NASA activities. Publications include final reports of major projects, monographs, data compilations, handbooks, sourcebooks, and special bibliographies.

TECHNOLOGY UTILIZATION PUBLICATIONS: Information on technology used by NASA that may be of particular interest in commercial and other non-aerospace applications. Publications include Tech Briefs, Technology Utilization Reports and Technology Surveys.

Details on the availability of these publications may be obtained from:

SCIENTIFIC AND TECHNICAL INFORMATION OFFICE

NATIONAL AERONAUTICS AND SPACE ADMINISTRATION

Washington, D.C. 20546